UNIVERSITY OF VERONA

Graduate School of Sciences Engineering Medicine
Ph.D. Program in Neuroscience

PhD THESIS

CHARACTERIZATION OF CELLULAR AND MOLECULAR MECHANISMS IN CELLULAR MODELS OF NEURONAL CEROID LIPOFUSCINOSES DISEASES

Coordinator:
Chiar.mo Prof. MICHELE TINAZZI

Tutor:
Chiar.mo Prof. ALESSANDRO SIMONATI

Student: MARIA CHIARA MESCHINI

XXVII CYCLE

Index

Introduction

1.1 Neuronal Ceroid Lipofuscinoses

The neuronal ceroid lipofuscinoses (NCLs) are a heterogeneous group of progressive neurodegenerative disorders affecting children and adults, characterized by retinopathy leading to blindness, ataxia and gait abnormalities, drug-resistant progressive myoclonic epilepsy, mental deterioration, and an early death. NCL diseases were classified according to the age at disease onset (congenital, infantile, late infantile, juvenile, adult). The NCLs have a worldwide distribution and are usually transmitted according to an autosomal-recessive pattern of inheritance. Fourteen different forms of NCL have been described to date, classified according to the designation of the mutated gene (*CLN*) and over 400 mutations have been identified (www.ucl.ac.uk/ncl/mutation). Many of the genes that cause typical NCL disease with onset in childhood have been identified and in very recent years the genetic basis of many of the later onset cases has been delineated, including the dominant adult onset NCL disease. More NCL genes remain to be identified as in some patients mutations cannot be demonstrated in any of the known NCL genes although they present with the typical NCL symptoms and characteristic lysosomal storage material (Tab.1).

Human neuronal ceroid lipofuscinoses variants					
Disease	**Eponym**	**OMIM**	**Clinical phenotype**	**Gene**	**Protein**
CLN1	Haltia–Santavuori	256730	Classic infantile, late infantile, juvenile, adult*	*CLN1* (*PPT1*)	PPT-1
CLN2	Janský–Bielschowsky	204500	Classic late infantile, juvenile*	*CLN2* (*TPP1*)	TPP-1
CLN3	Spielmeyer–Sjögren	204200	Juvenile*	*CLN3*	CLN3 protein (battenin)
CLN4	Parry	162350	Adult autosomal dominant*	*CLN4* (*DNAJC5*)	DnaJ homologue subfamily C member
CLN5	Finnish variant late infantile, variant juvenile (previously CLN9)	256731	Late infantile variant, juvenile, adult*	*CLN5*	Protein CLN5
CLN6	Early juvenile (Lake Cavanaugh), late infantile Costa Rican-Indian variant, adult Kuf type A	601780	Late infantile variant, adult* (Kuf, type A)*	*CLN6*	Protein CLN6
CLN7	Turkish variant late infantile	610951	Late infantile variant*, juvenile*, adult*	*CLN7* (*MFSD8*)	Major facilitator superfamily domain-containing protein
CLN8	Northern epilepsy, progressive EPMR	610003	Late infantile variant EPMR*	*CLN8*	Protein CLN8
CLN10	Congenital	610127	Congenital classic*, late infantile*, adult*	*CLN10* (*CTSD*)	Cathepsin D
CLN11	Adult variant	—	Adult*	*CLN11* (*GRN*)	Progranulin
CLN12	Juvenile variant	—	Juvenile, Kufor–Rakeb syndrome*	*CLN12* (*ATP13A2*)	—
CLN13	Adult Kuf type B	—	Adult Kuf type*	*CLN13* (*CTSF*)	Cathepsin F
CLN14	Infantile	—	Infantile, progressive myoclonus epilepsy 3*	*CLN14* (*KCTD7*)	Potassium channel tetramerization domain- containing protein
***These diseases have neurological involvement. Abbreviation: EPMR, epilepsy with mental retardation.**					

Table1. Human ceroid lipofuscinoses variants (Boustany et al., 2013).

They are considered lysosomal storage disorders (LSD), because of their characteristic accumulation of autofluorescent ceroid lipopigments, subunit

c of mitochondrial ATP synthase and/or the sphingolipid activator proteins saponins A and D (SAPs) in lysosomes of most cells, including neurons, skin fibroblasts and blood lymphocytes. Immunohistochemistry reveals the presence of abundant sphingolipid activator proteins (SAPs) in CLN1 and CLN10 whilst subunit C of mitochondrial ATP synthase (SCMAS) prevails in the lipopigments of other CLN forms. A minor component of either SAPs or SCMAS may also be encountered in the forms of CLN where the other component dominates the picture (Anderson et al., 2013). The various NCLs are characterized by electrondense ultrastructural features that are unique to each disorder, described as curvilinear (CV), rectilinear (RL), fingerprint (FP) or granular osmiophilic deposit (GROD) profiles, and the aberrant storage is accompanied by neuronal death and cerebral and/or cerebellar cortical atrophy (Anderson et al., 2013).

NCL-causing mutated proteins (CLN1 to CLN14) represent soluble lysosomal enzymes, polytopic membrane proteins which localize to the endoplasmic reticulum or to the endosomal/lysosomal compartment and directly or indirectly regulate lysosomal function (Fig.1). Although the precise function of most of the NCL proteins remains elusive. Despite the identification of several disease causing genes and many studies of the respective NCL proteins, the underlying pathological mechanisms remain obscure.

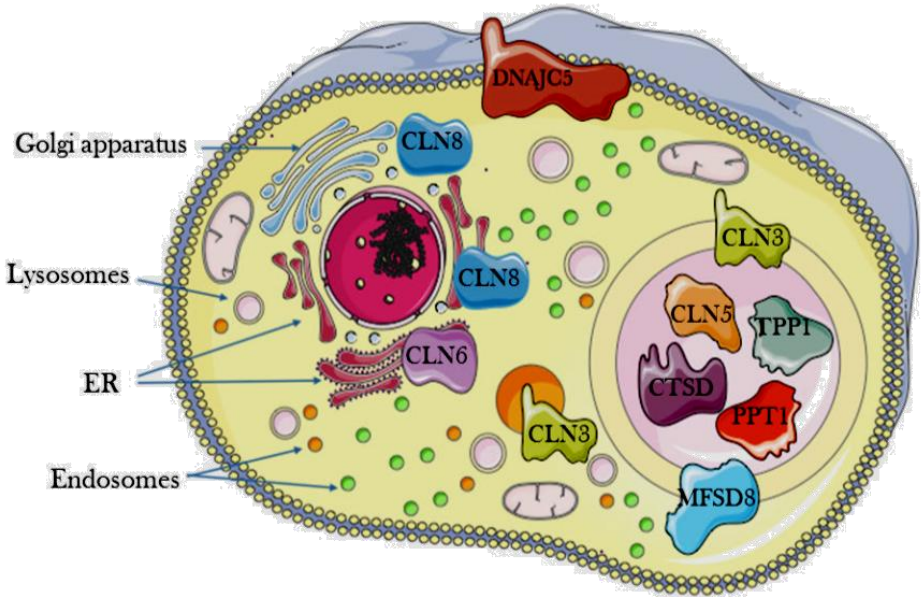

Figure 1. Hypothetical cellular localization of NCL proteins (This scheme was originally drawn by Dr. Marco Sardiello's laboratory) .

1.2 CLN1 Disease

Infantile neuronal ceroid lipofuscinosis (INCL, infantile Batten disease, or infantile CLN1 disease) (MIM#256730) is a rapidly progressing lysosomal storage disorder (LSD) caused by defects in the gene coding for palmitoyl protein thioesterase-1 (CLN1) (Vesa et al., 1995). This soluble lysosomal enzyme is responsible for cleaving long-chain fatty acid residues from cysteine residues on a multitude of protein targets. The CLN1 transcript is ubiquitously expressed; the nascent PPT1 polypeptide contains 306 amino acids, including a 25 amino acid signal sequence which is co-translationally cleaved (Camp et al., 1994). Mature PPT1 migrates as a ~37/35 kDa doublet, and is N-glycosylated at N197, N212, N232 in a manner essential for the activity, stability, and trafficking of the protein (Camp et al., 1994; Bellizzi et al 2000; Das et al. 2001; Lyly et al. 2007). The exact physiological function of PPT1 still remains elusive, but it is proposed that PPT1 participates in endocytosis, vesicular trafficking, synaptic function and cell death signaling and axonal guidance during

development. Lack of PPT1 activity can be used for diagnosis, in this case undegraded substrates accumulate in both CNS and systemic tissues. PPT1 is preferentially localized in cell soma and presynaptic terminals, including synaptic vesicles where it may serve a function specific to neuronal cells. Invariably mutations in PPT1/*CLN1* are associated with granular appearance of stored material (granular osmiophilic deposits, GRODs). Most mutations are missense and affect residues conserved in diverse species. Nonsense mutations or mutations causing frame-shift that result in premature truncation of PPT1 are predicted to lead to total loss of enzymatic activity. Many of the CLN1 mutations are private but two mutations appear with greater frequency: c.364A>T resulting in R122W is frequently found in patients of Finnish ancestry, and c.451C>T (R151X) has been identified in a more global population of less defined ancestry. These two mutations represent about 20% each of the total abnormal *CLN1* alleles. Recently, a structural basis for the effect of CLN1 mutants was constructed showing that mutations associated with a total loss of enzymatic activity affect the core region of the enzyme, whereas less severe mutations are localized at the surface of PPT1 (Ohno et al., 1997). The clinical spectrum of CLN1 disease is extremely wide, with age at onset varying from infancy to adulthood. The majority of patients are diagnosed as infantile-onset NCL, with manifestations in the second half of the first year of life in the form of seizures, mental decay, loss of vision and brain atrophy. In patients with this NCL form, early development appears normal until 6–18 months of age. At on set, there is typically decreased tone and decreased social interaction followed by rapidly progressive psychomotor regression, myoclonus, seizures, and visual failure. By 2 years of age, there is blindness with optic atrophy and macular and retinal changes but no pigment aggregation. Progressive brain atrophy is accompanied by a flat electroencephalogram. There is also early extinction on the electroretinogram. Seizures in infantile NCL may not be as prominent as in later-on set forms. Ultimately, spasticity develops and patients become vegetative. Fewer cases are seen with onset of symptoms in later childhood

(Simonati et al., 2009), adolescence (Perez-Poyato et al., 2011) and even in adulthood (Ramadan et al., 2007). Regardless of the age at onset and clinical features, the presence of low-absent PPT1 activity and the ultrastructural evidence of GRODs are hallmarks of proteolipidic storage in all phenotype. The mechanism by which decreased PPT1 activity leads to the formation of GRODs remains to be clarified.

Two mouse models of infantile CLN1 disease were initially developed that are completely deficient in PPT1 activity (Gupta et al. 2001; Jalanko et al. 2005). More recently, a novel *Cln1*^{R151X} knock-in model has been produced (Miller et al., 2015). These animals recapitulate many features of the human disease including progressive neurodegeneration, cortical thinning, brain atrophy, autofluorescent accumulation, retinal dysfunction, spontaneous seizures, motor deficits and shortened lifespan (Bible et al. 2004; Griffey et al. 2005; Gupta et al., 2001). In addition, immunohistochemical staining for GFAP and CD68 showed reactive changes in astrocytes and microglia cell populations, respectively. Astrocytosis has been reported in almost all forms of human NCL (Haltia et al., 1973). This process mediates how neurons respond to injury, and may also influence neuronal function through direct effects upon the synaptic environment (Bible et al., 2004). There is growing evidence that the activation of astrocytes within the thalamus precedes neuronal cell loss (Bible et al., 2004). However, it is still unclear whether astrocytosis directly affects neuronal cell loss in the cortex, or if it is a downstream consequence of the disease process. The expression of PPT1 in mouse brain preparations and cultured neurons parallels with the abundance of presynaptic marker protein and indicates a role for PPT1 in synaptogenesis (Isosomppi et al., 1999; Ahtiainen et al., 2003), implicated in the recycling of synaptic vesicles. The localization of PPT1 in synaptic vesicles, however, is a matter of debate (Heinonen et al., 2000; Lehtovirta et al., 2001; Virmani et al., 2005). The difference in processing and trafficking of PPT1 between non-neuronal and neuronal cell types further highlights putative distinct functions of PPT1 in neurons (Lyly et al., 2007). Several

studies found that changes in the levels of PPT1 expression correlated with the activation of caspase-mediated apoptotic pathways in neuroblastoma cells and lymphoblasts (Cho et al., 2000; Cho et al., 2000; Zhang et al., 2001), which appear to be caused by ER and oxidative stress (Kim et al., 2006; Kim et al., 2006; Zhang et al., 2006). PPT1 has been repeatedly associated with lipid metabolism. Post- mortem brain samples of CLN1 disease patients revealed changes in phospholipid content. Ceramide levels of lipid rafts have been reported to be decreased in CHO cells overexpressing PPT1 most likely due to the fact that PPT1 is involved in the processing of saposin D, a storage component in CLN1 disease, and involved in ceramide catabolism (Goswami et al., 2005; Ahtiainen et al., 2006). Moreover, early infiltration of CD8 + T-lymphocytes and an activation of microglia/macrophage-like cells associated with progressive degeneration and loss of retinal ganglion cells was seen in the $Ppt1^{-/-}$ model (Groh et al., 2013).

A recent study have outlined the spatial relationship between lysosomal engulfment and damaged mitochondrial reticulum in CLN1 fibroblasts, and have demonstrated that the mitochondrial compartment is affected in these cells *in vitro*. Abnormalities in the number, intracellular localization pattern and morphology of mitochondria, as well as defects in the mitochondrial enzyme activities and adaptive energy metabolism have been observed in patient fibroblasts. These results are in agreement with previous studies in sheep, $Ppt1^{-/-}$ mice, and Caenorhabditis elegans (Das et al., 1999; Pezzini et al., 2011; Porter et al., 2005; Wei et al., 2011). Additional investigations on alterations of the mitochondrial compartment in neuronal cells could reveal new insights into the cell pathology of the severe CLN1 encephalopathy of childhood.

Several therapeutic strategies including enzyme replacement, gene therapy, stem cell-mediated therapy, and small molecule drugs have resulted in minimal to modest improvements in the murine model of PPT1-deficiency. However, more recent studies using various combinations of these approaches have shown more promising results; in some instances more

than doubling the lifespan of PPT1-deficient mice. These combination therapies that target different pathogenic mechanisms may offer the hope of treating this profoundly neurodegenerative disorder (Hawkins-Salsbury et al., 2013).

1.3 CLN5 disease

The CLN5 form is a variant late infantile subtype of NCL (MIM# 256731) originally described in Finland, where a founder p.Tyr392* mutation occurs, and later observed on different ethnicities. In Italy, up to 6% of the identified NCL cases harbor mutations in *CLN5*. Onset of the disease is usually at 4–7years of age, though rare cases may start in the juvenile period or even in adulthood and manifest with motor clumsiness, language delay, progressive visual impairment, and ataxia (Santavuori et al., 1992; Santavuori et al., 1993; Holmberg et al., 2000; Mancini et al., 2015). As the disease progresses, myoclonus, epileptic seizures, and further mental and motor deterioration develop (Santavuori et al., 1991). Affected children become blind within 10 years from disease onset, and death usually occurs between 10 and 30 years. There is a lag between birth and onset of symptoms and in developing blindness that should be weighted as a possible therapeutic window if we had the appropriate strategy. Pathologically, the CLN5 storage material is made of subunit c of the mitochondrial ATP synthase and accumulates in different tissues with curvilinear bodies and fingerprint-like structures evidenced at ultrastructure (Tyynelä et al., 1997).

The *CLN5* gene encodes a protein (CLN5p) that has a 46 kDa predicted molecular mass and no sequence homology to other proteins (Savukoski et al., 1998). CLN5p contains a signal peptide (SP) that is cleaved in the endoplasmic reticulum (ER) and the mature polypeptide is mainly localized in lysosomes, but the full topology of CLN5p is not known. Mature CLN5p has mostly been reported to be a soluble protein based on the fact that it is secreted, and that it contains mannose-6-phosphate (M6P) residues but its

solubility versus membrane-spanning property has been a controversial issue (Holmberg et. Al, 2004; Isosomppi et al., 2002; Schmiedt et al., 2010; Vesa et al., 2002). Mutations in *CLN5* have been reported to prevent trafficking of CLN5p to the level of ER (Lebrun et al., 2009) and Golgi (Isosomppi et al., 2002) but also not dramatically affect trafficking to the lysosomes (Schmiedt et al., 2010). CLN5p has also been shown to be a highly glycosylated soluble lysosomal protein and three of the eight potential N-linked glycans at N320, N330 and N401 contain M6P residues (Schmiedt et al., 2010; Lebrun et al., 2009; Kollmann et al., 2005; Sleat et al., 2006). Recent studies have proposed CLN5p as controlling the itinerary of the lysosomal sorting receptors by regulating retromer recruitment at the endosome (Mamo et al., 2012) likely because of the possible interactions of CLN5p with several other NCL proteins including PPT1/CLN1, TPP1/CLN2, CLN3, CLN6 and CLN8 (Isosomppi et al., 2002; Schmiedt et al., 2010). Murine Cln5 has a prominent homology to human CLN5; Cln5 knockout mouse develops typical symptoms of an NCL disease (Holmberg et al., 2004; Kopra et al., 2004). Loss of Cln5 in mice leads to defective myelination in vitro and in the developing brain; this is accompanied by a defective sphingolipid transport (Schmiedt et al., 2012). In double knockout mice (Cln1/5 double-ko) comparative gene expression profiling in brain has suggested common defective pathways linked to neuronal growth cone stabilization (Blom et al, 2013). It has also been observed a pronounced accumulation of autofluorescent storage material, and an alteration in lipid metabolism (specific increase in plasma phospholipid transfer protein activity) with prominent downregulation of α-synuclein in mouse brains. CLN5-deficient patient fibroblast cells manifest increased apoptosis with very low ceramide levels; addition of CLN8p (the product of an additional NCL gene) or CERS1 (ceramide synthase) (that has been recently associated with myoclonus epilepsy and dementia in a kindred [Vanni et al., 2014]) brings correction to this phenotype (Schulz et al., 2006). The fibroblasts of Cln8-deficient mouse model (Cln8mnd) show not only decreased activity of ceramide synthase but also reduced levels of

ceramide produced by CERS1, a finding very similar to what is seen in the CLN5 mutant cells (Haddad et al., 2012) and explaining the ability of CLN8p overexpression to complement the CLN5 pathological phenotype.

In mammals, ceramide represents a central molecule of sphingolipid metabolism, implicated in cell signaling, growth, proliferation, differentiation, apoptosis, and autophagy. Ceramide is synthesized by a family of six synthases (CerS1 to CerS6), each of which utilizes distinct acyl chain lengths varying from C14 to C26. In the central nervous system (CNS), the most highly expressed ceramide synthase is CerS1, which is particularly expressed in neurons of neocortex, hippocampus, and cerebellum. CerS1, a transmembrane protein located in the cytosolic leaflet of the ER membrane, shows distinctive specificity for (dh)C18-acylCoA and represents the main catalyzer of C18 (dh)ceramide synthesis in the brain. However, the specific function of C18-ceramides — and of other sphingolipid subtypes — is still largely unknown (Levy et al., 2010).

Alike CLN8p, all mammalian CerS share a distinct domain, the Tram-Lag-CLN8 (TLC) domain, a region of ~200 residues also found in other proteins. Lipidomic analysis of brain samples from CLN8 patients showed reduced levels of ceramide, as well as a decrease in long fatty acyl chain containing molecular species within the sphingolipids (Hermansson et al., 2005). All together these data suggests that CLN8p and CLN5p may act in a concerted manner with Cers1 in ceramide synthesis. Intriguingly, some of ceramides modulate mitochondrial function and oxidative phosphorylation (OxPhos) as they suppress respiratory chain activity, induce ROS production and oxidative stress, regulate mitophagy, disrupt the mitochondrial membrane potential, and induce mitochondrial outer membrane permeabilization (MOMP) and possibly apoptosis. Recently a mechanistic link has been established between C18-ceramide produced by CerS1 and the induction of mitophagy, suggesting a clue for the involvement of Cers1 in neurodegeneration (Sentelle et al., 2012). Mitochondrial ceramide directly binds and recruits LC3B-II labeled autophagosomes to damaged mitochondria for lysosomal degradation, a

condition also termed lethal mitophagy. In fact, generation of C18-ceramide by CerS1 and ceramide localization to mitochondria were required for stress-induced lethal autophagy/mitophagy, which was Drp1-mitochondrial fission dependent, placing mitochondrial ceramide in the center for selectively inducing lethal mitophagy.

1.4 CLN13-Kufs Disease

Kufs disease (KD), the most common form of adult NCL, is the least frequent and most difficult to diagnose; the symptoms can be vague and difficult to sort out among a variety of other disorders (Cotman et al., 2013). Diagnostic difficulties have delayed discovery of the molecular defects underlying adult NCLs. The first genes implicated in KD were reported in 2011. KD can present as the Type A form, characterized by progressive myoclonus epilepsy or Type B, with movement and behavioral abnormalities and dementia (Berkovic et al., 1988). Mutations in *CLN6* represent the major cause of autosomal recessive Type A KD whereas variants in *DNAJC5* are associated with the autosomal dominant form of the disease- Parry disease (Williams et al., 2012). Cathepsin F (*CTSF*, *CLN13*) mutations have recently been discovered in autosomal recessive Type B KD families of French-Canadian, Australian, and Italian origin (Smith et al., 2013). The slow progression rate of the disease is also observed in cathepsin F-deficient mice showing a late onset accumulation of autofluorescent lipofuscin throughout the CNS (Tang et al., 2006).

CTSF is a widely expressed in human tissues with high levels in the heart, brain, skeletal muscle, testis, and ovary; it is a lysosomal cysteine protease whose role in vivo is unknown. Cathepsin F is the only cysteine cathepsin whose inactivation alone results in a lysosomal storage defect and progressive neurological features in mice. CTSF protein consists of 484 amino acids. After cleavage of a 19 residue signal peptide CTSF is modified on oligosaccharides linked to N378 and N440 with M6P-residues (Sleat et al., 2006). Of the eleven human cysteine cathepsins, cathepsin F is

the only cathepsin that exhibits an extended N-terminal proregion (251 amino acid), which contains a cystatin-like domain and it might function as an endogenous cysteine protease inhibitor (Santamaria et al., 1999; Wang et al., 1998; Wex et al., 1999). Over-expression of N-terminus truncated forms of human cathepsin F (Δ-CtsF) in HEK 293T cells have recently been associated with features suggestive of aggresome-like inclusions, inducing autophagic features (Jerič et al., 2013). In the work in question, the truncated forms of human cathepsin F appeared to be co-localized with aggresome-related proteins such as p62/sqstm1, a multifunctional polyubiquitin-binding protein commonly seen in diseases with protein aggregation.

CTSF is synthesized as an inactive preproenzyme that may be targeted to the endosomal/lysosomal compartment via the M6P-receptor pathway. The physiological function of CTSF is still unclear; but analysis of Ctsf-deficient mice and in vitro studies indicated that this lysosomal cysteine protease is involved in degradation of class II-associated invariant chain peptide and MHC class II peptide loading (Shi et al., 2000), lipoprotein degradation, potentially linked to the formation of atherosclerotic lesions (Tang et al., 2006; Lindstedt et al., 2003; Oörni et al., 2004, angiogenesis and tumor-associated inflammation (Smith et al., 2012). Recently, the heterologous expression and *in vitro* studies suggest that cathepsin-F is mainly responsible for the lysosomal processing of wild-type lysosomal integral membrane protein type-2 (LIMP-2) (Peters et al., 2015). Lack of LIMP-2 cleavage may contribute to the pathogenesis of type-B-Kufs-disease by impaired lysosomal degradation, leading to a reduced autophagic flow and accumulation of engulfed structures, a hallmark of many NCLs (Lieberman et al., 2012).

Aims

The overall aim of this research project was to investigate the cellular and molecular mechanisms underlying three different forms of NCLs disease using patients' material and cell models. The reasons to investigate CLN1, CLN5, and CLN13 is three-fold. First, both CLN1 and CLN5 are relatively frequent among the forms in the Italian NCL cohort and the molecular pathogenesis is less clear than the other forms such as CLN3 and CLN6. Second, the Center where this work was largely undertaken (Simonati's laboratory, "Developmental Neuropathology"; Department of Neurological, Psycological, Morfological and Motor Sciences, University of Verona) has gained over the past decade a specific expertise in the clinical, pathological, and molecular definition of children carrying the CLN1 or the CLN5 disease and sufficient biological material was available in the laboratory biorepository. Third, the exciting identification of a novel disease variant in the Italian group of NCL patients (i.e., CLN13) demanded for the use of the tools we had developed in CLN1 and CLN5 to further investigate the molecular mechanisms.

Thus, the specific objectives of my PhD work were:

1. To study the cell pathology caused by Mediterranean *CLN1* mutations implicated in Infantile neuronal ceroid lipofuscinosis (INCL-*CLN1*), we used human skin fibroblasts of CLN1 patients and derived cultured neuroblastoma cells. We tested mitochondrial structure and functions in these cells, aiming at the identification of biomarkers of CLN1 disease. Human neuroblastoma cells (SH-SY5Y) are an excellent system *in vitro* and provide an invaluable experimental tool for investigating the molecular pathophysiology of NCL disorders in neuronal cell. In this regard, SH-SY5Y are also valuable because of unlimited proliferation and the ability to differentiate into human neuron-like cells. Furthermore, these model

systems will offer an opportunity to test *in vitro* therapeutic and pharmacological treatments to modulate mitochondrial functions.

2.To test the hypothesis that CLN5p (the product mutated in Variant late infantile subtype of NCL, vLINCL-*CLN5*) can be functionally related with CerS1 and CLN8p. We studied if such association could also promote dysregulated sphingolipid metabolism in disease conditions and if it is associated with mitochondrial dysfunction ultimately leading to a neurodegeneration. The first objective was to explore the role of the CLN5p in terms of functional interactions between CLN5, the lysosomal proteins and ceramides, using a cell model system. A second aim was to investigate the mitochondrial bioenergetics in patient-derived fibroblasts.

3. To characterize at the cell level of a novel mutation in *CTSF* associated with Adult NCL- Type B Kufs diseases (*CLN13*). We investigated the putative role of a new N-terminally truncated form of Cathepsin F protein in human fibroblasts in terms of protein aggregation and lysosomal storage.

Use of different cell types permitted for the first type a finer study of molecular interaction in CLN5 pathogenesis, the first ever molecular investigation in CLN13 disease, and an innovative comparison between patients' derived material and cellular models (developed in Simonati's laboratory) in CLN1 disease.

Results

2.1 Mediterrean CLN1 mutations are associated with mitochondrial dysfunction

In this study we have used an *in vitro* system of human neuroblastoma cells, SH-SY5Y, reproducing the pathological features observed in "Mediterranean" *CLN1* mutations. In such cells, we modeled the missense mutation c.665T>C (L222P) which reduces the PPT1 activity and the in-frame deletion of the second exon (c.125_235del) which predicts loss of important residues for protein folding and predicts an unstable gene product degraded (Simonati et al., 2009).

We investigated the mitochondrial and cellular consequences comparing results with the corresponding patient's mutated fibroblasts cell lines.

To get further insights on the role and functions of the CLN1 protein, we studied representative gene mutations that are present in a larger group of Italian patients affected by classical and variant CLN1-disease (Santorelli et al., 2013). We conducted our experiments in primary cells lines (skin fibroblasts) derived from patients and in stably transfected clones over-expressing the wt and mutated cDNAs. In particular we considered the deletion of the second exon (c.125_235del) in which the ORF is maintained (Santorelli et al., 1998), but the deletion might cause loss residues needed for correct protein folding. Hence, the specific mutation might cause severe biochemical defect through protein degradation (Simonati et al., 2009) . We also studied a missense mutation, namely, the c.665T>C/L222P, which reduces PPT1 enzyme activity. In order to verify the extent of over-expression of wt and mutated cDNAs, we initially performed immunocitochemistry using PPT1 antibody (Fig.2).

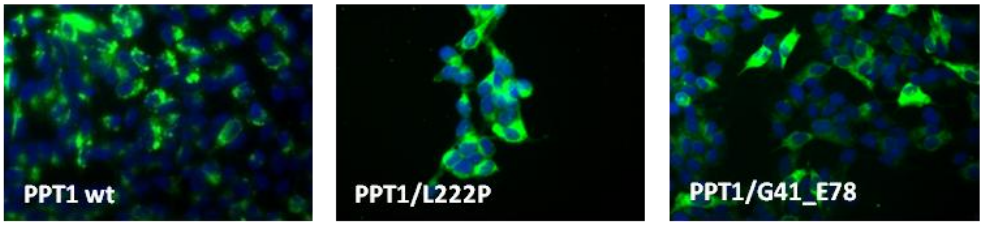

Figure 2. Stable transfection in SH-SY5Y cells that over-express PPT1 wt and mutated. Immunocytochemistry experiments show the results of PPT1 expression level in engineered SH-SY5Y cells. PPT-1 is evidenced in green and nuclei are counterstained with DAPI.

2.1.1 Analysis of mitochondrial compartment in CLN1 fibroblasts

In the first part of the study we evaluated the effects of lysosomal storage on the mitochondrial compartment in primary mutant CLN1 skin fibroblasts, focusing on the structural changes of the mitochondrial reticulum. We put attention on two Mediterranean *CLN1* mutations, that is, c.124+1215_235-102del3.6Kb /p.A43_G145del (variant late-infantile) and c.665T>C/p.L222P (juvenile). In primary cells, we observed a fragmentation of the mitochondrial network as depicted by porin (VDCA) staining. We observed a prevalence of punctuate profile in fibroblasts as compared to the regular network of control cell lines which under normal condition forms a tubular, regular reticulum, mainly distributed around the nuclei, confirming an alteration of the mitochondrial network, as already reported (Pezzini et al. 2011). The capacity of patients' fibroblasts to support oxidative phosphorylation was examined by measuring cellular ATP production *in vitro* using a luminometric assay. Fibroblasts were cultured with glucose (G) or under conditions that supported only glycolytic (glucose with oligomycin, G+O) or mitochondrial ATP production (2-deoxy-D-glucose with pyruvate, D+P). Under oxidative conditions the ATP levels were significantly reduced in the patients compared to control values. (Fig.3)

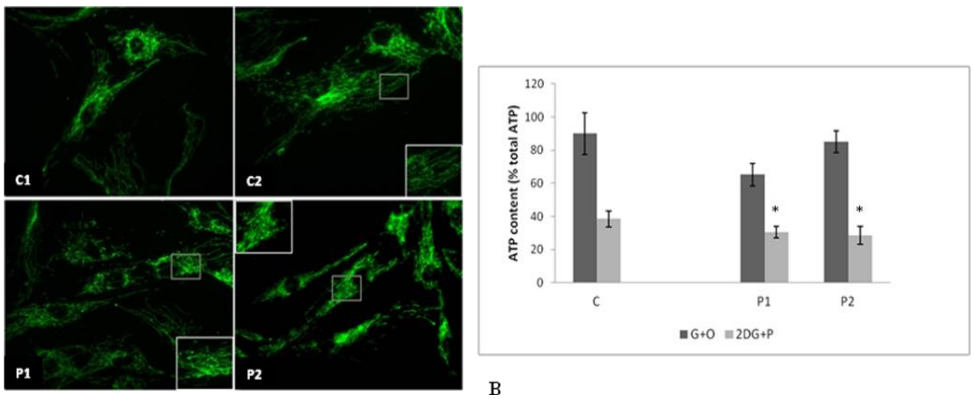

B

Figure 3. Mitochondrial morpho/functional analysis in fibroblasts. A: mitochondrial features of the mitochondrial reticulum (as depicted by Porin staining) in CLN1 cells. B: cells were incubated 2 h in ATP record buffer supplemented with 10 mM glucose (Glu), 2.5 mg/mL oligomycin (Oligo), and 5 mM 2-deoxy-D-glucose plus 5 mM pyruvate (2GD+Pyr).
P1: p.L222P; P2: p.V181L/p.A43_G145del. * P value< 0.005.

2.1.2 Differentiation of CLN1 neuroblastoma stable clones

To assess the functional effect of the two different mutations in *CLN1* (p.A43_G145del and p.L222P), we obtained cells featuring mature neuron-like structures from stable SH-SY5Y cells line overexpressing the mutations. We differentiated clones with stable transfection upon exposure to retinoic acid for 6 days (pre-differentiation phase), and we then used a enriched neurobasal medium for 3 days (differentiation phase). On parental SY5Y cells we observed an increased number of long axonal processes (βIII tubulin marker; Fig.4A) and an increase of βIII tubulin expression level (Fig. 4B). Moreover, we demonstrated that stable *CLN1* clones were able to differentiate after combined treatment with RA and neurobasal medium, as demonstrated by the increase expression of some neuronal markers (Fig. 4C). In conclusion, the neuronal model generated was able to mimic neuronal features and could generate a model to go inside the pathological mechanism of the neurodegenerative disease.

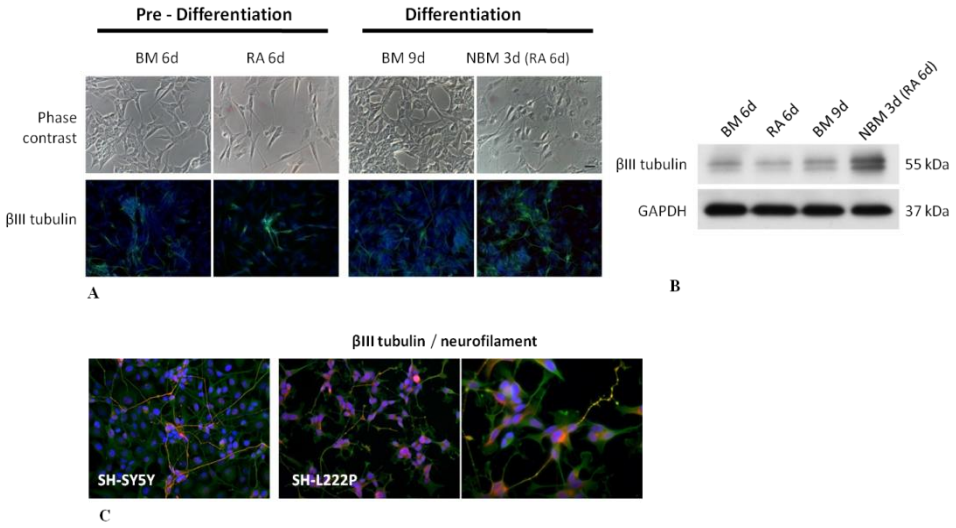

Figure 4. Differentiation experiment upon exposure to retinoic acid for 6 days (Pre differentiation phase), and then to neurobasal medium for 3 days (Differentiation phase). A: Immuonofluorescence for βIII tubulin (green) and nuclei are counterstained with DAPI. B: Western blotting on parental SH-SY5Y cells using βIII tubulin antibody. C**:** stable SH-SY5Y cells line wt and overexpressing the L222P mutation treated with NBM showed an increase in neurite outgrowth (green: βIII tubulin; red: SMI31R antibody, specific for heavy chain neurofilaments).

2.1.3 Analysis of mitochondrial compartment in CLN1 neuroblastoma stable clones

We analyzed the mitochondrial functions in differentiated SHSY5Y wild-type and stably transfected cells harboring mutations in *CLN1* (p.A43_G145del and p.L222P). The study of mitochondrial network with a porin antibody showed mitochondrial fragmentation in the p.L222P clone (Fig 5A). The oxidative ATP production was comparable in the different cells lines (Fig. 5B) whereas the complex I and complex IV activities, evaluated by BN-IGA, showed an increase in the mutant clones when compared with SHSY5Y cells. Western blotting using antibodies against different subunits of respiratory chain complexes revealed normal steady state levels of all subunits (Fig. 6A-B).

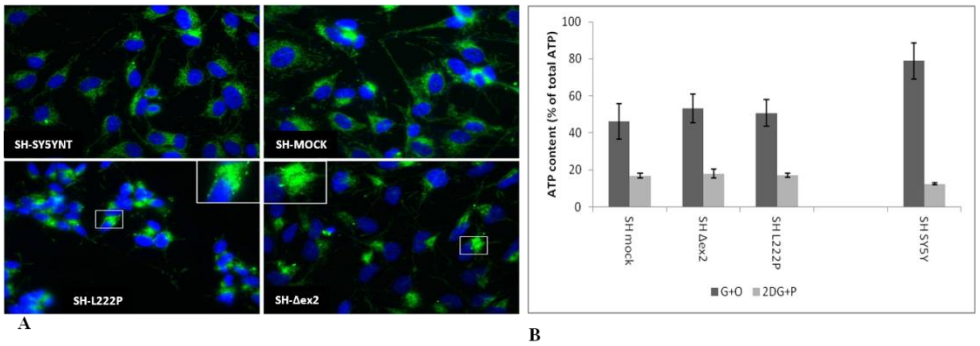

Figure 5. Mitochondrial morpho/functional analysis in differentiated stable clones A: mitochondrial features of the mitochondrial reticulum (as depicted by Porin staining) in CLN1 cells. B: cells were incubated 2 h in ATP record buffer supplemented with 10 mM glucose (Glu), 2.5 mg/mL oligomycin (Oligo), and 5 mM 2-deoxy-D-glucose plus 5 mM pyruvate (2GD+Pyr).

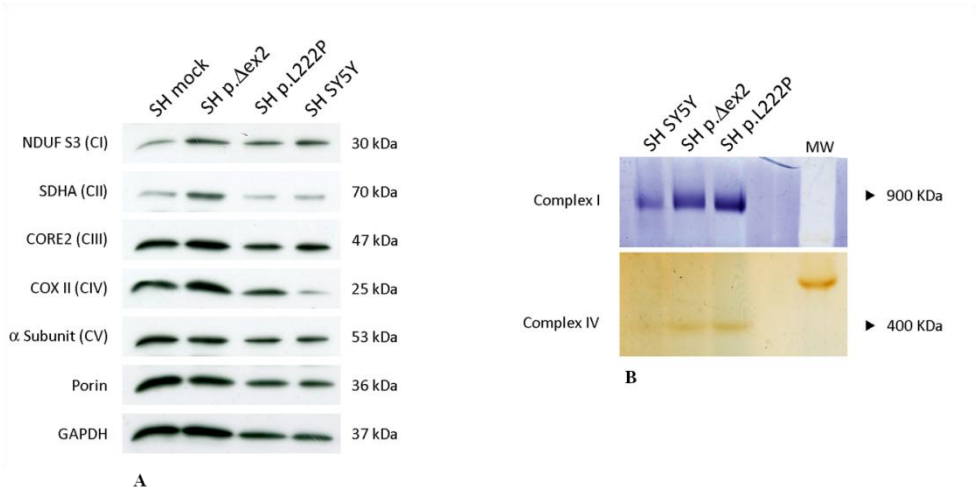

Figure 6. Expression of mitochondrial proteins in differentiated stable clones A: cell lysates were separated by SDS-PAGE, and analyzed with specific antibodies against different subunits of respiratory chain complexes. Porin and GAPDH were used as control for equal loading. B: In gel activity assay of complex I and IV in native conditions.

2.2 CLN5 is a partner of ceramide synthase enzymes

We investigated the pathogenetic mechanism underlying the CLN5 disease, a rare form of Neuronal Ceroid Lipofuscinoses (NCLs), a variant accounting for up to 6% of the Italian NCL population.

We studied the functional interactions between CLN5, the lysosomal proteins and ceramides, using different approaches in a cell model system; and analyzed the mitochondrial bioenergetics in patient-derived fibroblasts.

2.2.1 Interactions of CLN5 with other NCL proteins and ceramides

The possible interactions of CLN5 with other NCL proteins, lysosomal hydrolases and ceramides were investigated in appropriate cellular systems. We performed bimolecular fluorescence complementation (BiFC) analysis in HeLa cells to visualize the direct interactions of proteins in living cells. The BiFC assay is based on two non-fluorescent fragments of a fluorescent protein which, when fused to two interacting proteins, yield fluorescence due to the stable formation of a functional fluorescent protein inside the cell. We created construct plasmid expression vectors, using the appropriate vectors, by fusing the sequences encoding the selected fluorescent protein fragments (YFP - yellow fluorescent protein) with the sequences encoding the proteins of interest and expressed them in HeLa cells. Morover we tested the interactions between CLN5 constructs Y1-Y2 and a library plasmids of lysosomal proteins (Tab.2). The protein interaction was visualized and quantified by confocal microscopy (Fig.7A) and Flow Cytometric Analysis (FACS) (Fig.7B). We observed a significative interaction between CLN5p and CLN8p and of CERS proteins (Cers1, 2, 4, 5).

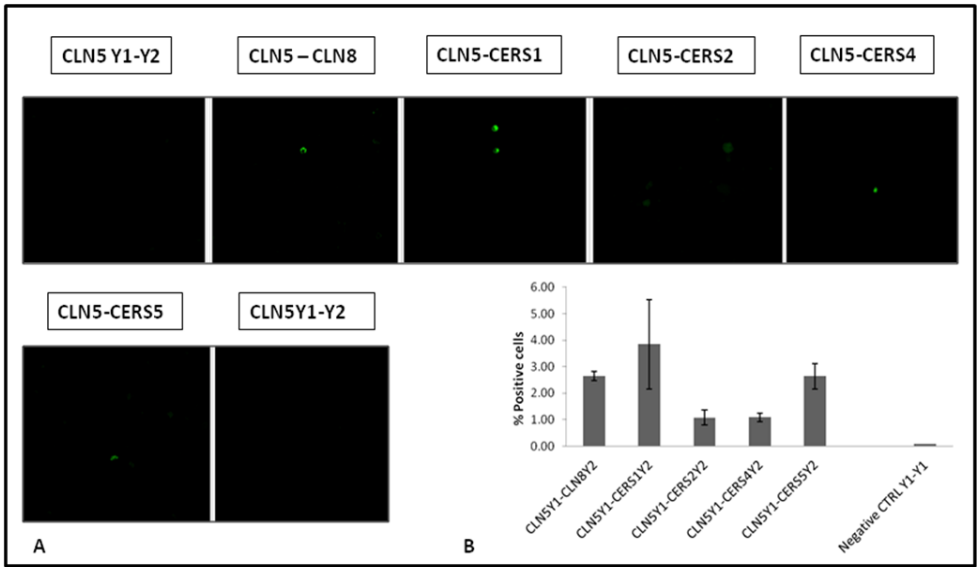

Figure 7. BiFC analysis. A) Confocal microscopy: pCLN5-YFP1-YFP2, pCLN8-YFP2, pCERS1-YFP2, pCERS2-YFP2, pCERS4-YFP2, pCERS5-YFP2 and pCERS6-YFP2 were transfected into HeLa cells and cultured in normal condition. Fluorescence intensities of BiFC (green). B) FACS: percentage of Hela cells positives for the interactions.

We also confirmed these interactions using co-immunoprecipitation in HeLa cells by transfecting FLAG, MycC and YFP-tagged proteins (Fig.8A-D). A CLN5-Myc fusion protein expressing in HeLa was used to pull down the other proteins. The pull downs were prepared from lysates of HeLa cells transiently transfected with different CLN8 and ceramide synthase proteins (CERS2,4, 5, and 6) (Fig.8A-D). The bound proteins were identified by Western blotting analyses.

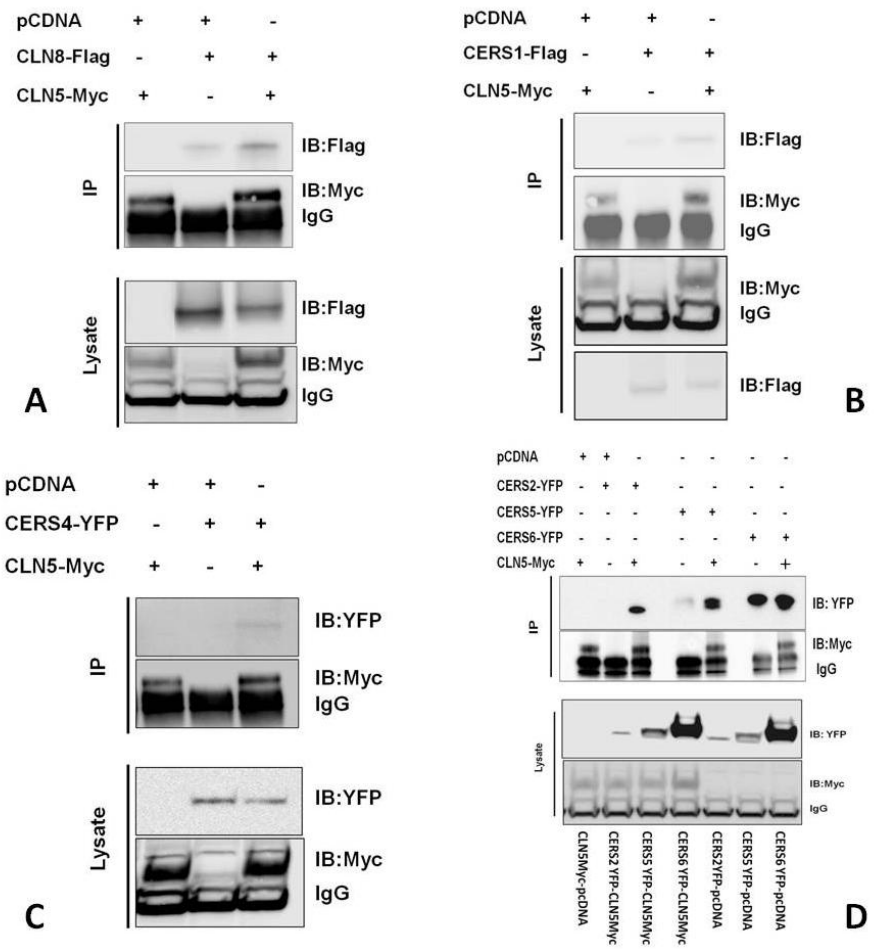

Figure 8. Co-Immunoprecipitation. Interactions of CLN5 with other NCL proteins. The Cln5-cDNA was expressed as Myc fusion protein and used to pull down proteins from HeLa cell lysates. CLN8 (A), CERS1-c-FLAG (B), CERS4-YFP (C) and CERS5, CERS6-YFP (D). The bound proteins were immunoblotted and detected with specific antibodies listed in Methods section.

2.2.2 Intracellular localisation of CLN5 and ceramide synthases proteins

Double immunofluorescence microscopy of HeLa cells transfected with CLN5 cDNA-YFP showed complete colocalisation of CLN5 protein with the endoplasmic reticulum (ER) marker PDI, whereas no colocalisation was detected with the marker protein of the late endosomal/lysosomal protein LAMP2 (Fig.9).

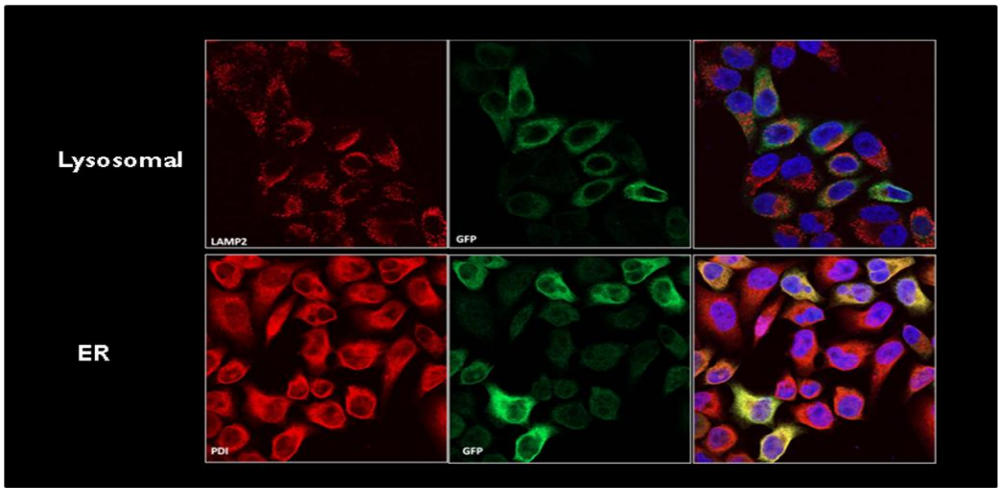

Figure 9. HeLa cells were transiently transfected with CLN5. Twenty-four hours after transfection, cells were fixed and subsequently stained with the GFP antibody (green), LAMP2, the ER marker protein PDI (all in red). Merged images indicate overlapping localisation (yellow). Nuclei (blue) were visualized by staining with DAPI.

Again, double immunofluorescence microscopy of HeLa cells transfected with CERs cDNA-YFP (CERS1, CERS2, CERS4, CERS5, CERS6) showed complete colocalisation of CLN5 protein with the ER marker PDI, whereas no colocalisation was detected with the marker protein of the cis-Golgi (GM130) (Fig.10).

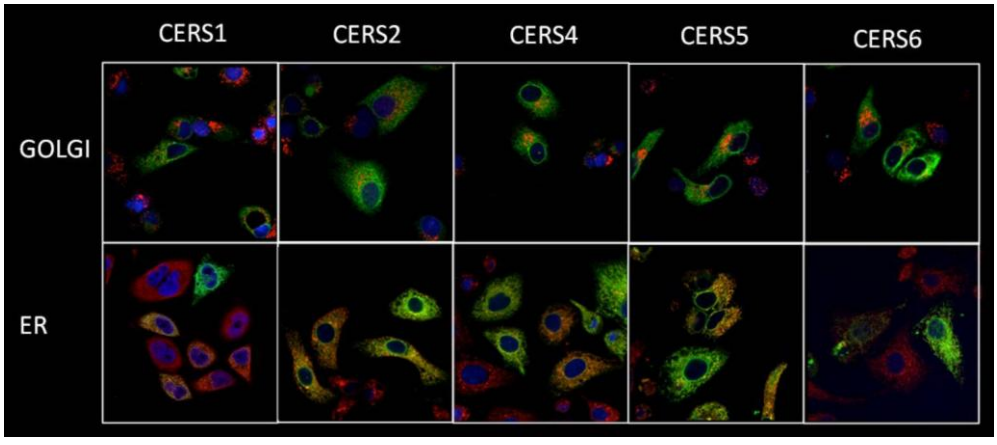

Figure 10. HeLa cells were transiently transfected with CERSs. Twenty-four hours after transfection, cells were fixed and subsequently stained with the GFP antibody (green), the Golgi protein GM130, the ER marker protein PDI (all in red). Merged images indicate overlapping localisation (yellow). Nuclei (blue) were visualized by staining with DAPI.

2.2.3 Analyses of intracellular trafficking of CLN5 together with the CLN8 interacting protein

To dissect the role of CLN5p interaction with CLN8p *in vitro*, we transiently co-transfected HeLa cells with the CLN5-Myc and CLN8-FLAG constructs. In the second series of experiment we studied the CLN5-Myc localization after the silencing with SiRNA CLN8. We observed the specific presence of CLN5-Myc in ER compartment in the both conditions (Fig.11). The interaction between CLN5p, ER resident proteins and CLN8p, occur in the ER, and the presence of CLN5p in that compartment is independent of the CLN8p presence.

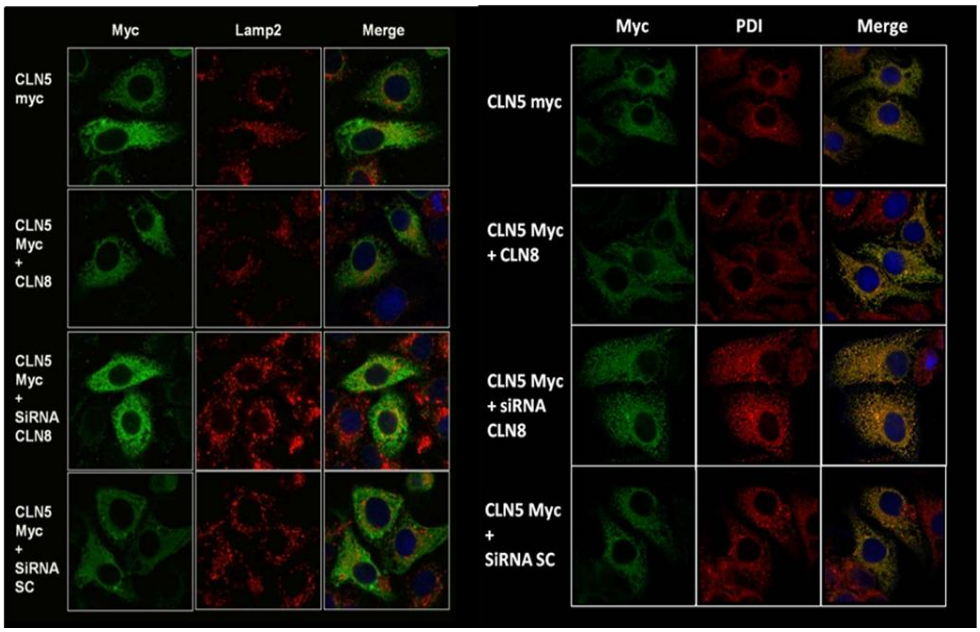

Figure 11. Consequences in HeLa cells of deficiency of the ER-resident trafficking protein CLN8 on the localization of CLN5. HeLa cells were transiently transfected alone with the CLN5 (CLN5-Myc) or together with CLN8 FLAG, SiRNA CLN8 and SiRNA SC. The cells were fixed with methanol 24 h post transfection, stained with the Myc (green), the lysosomal protein (LAMP2) and the ER marker PDI (all in red). Merged images indicate overlapping localisation (yellow). Nuclei (blue) were visualized by staining with DAPI.

To better investigate the role of CLN8 in CLN5 trafficking, we transfected MEF cells from wild type and CLN8 deficient ($Cln8^{-/-}$) mice with CLN5-Myc. In these murine cells CLN5p we confirmed the results obtained in HeLa cells (Fig. 12).

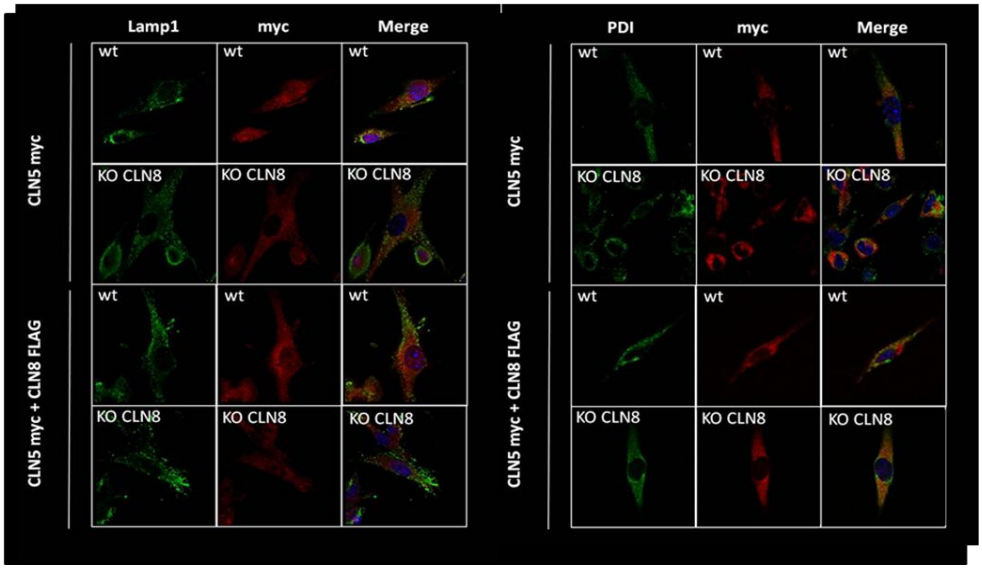

Figure 12. MEF cells were transiently transfected alone with CLN5 (CLN5-Myc) or together with CLN8 FLAG. The cells were fixed with PFAl 24 h post transfection, stained with the Myc (red), the lysosomal protein (LAMP1) and the ER marker PDI (all in green). Merged images indicate overlapping localisation (yellow). Nuclei (blue) were visualized by staining with DAPI.

2.2.4 Lysosomal enzyme activities in CLN5 fibroblasts

We performed the fluorimetric activities of different lysosomal enzymes, causing others forms of lysosomal storage disorders, in wild-type and *CLN5* patient's fibroblasts (c.595C>T /p.R99*) primary fibroblast.

We measured the activities using specifics substrates, we observed a significant reduction of TTP1 (*CLN2*) and β-galactosidase 1 (*GLB1*) (Fig.13A-B).

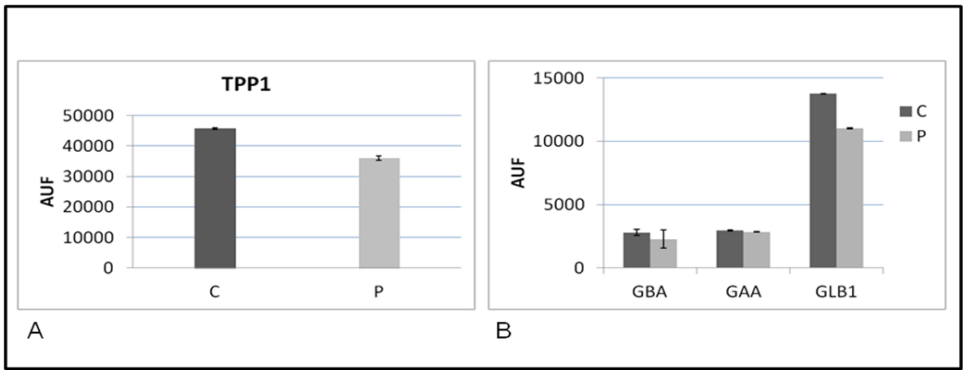

Figure 13. Enzyme activities. Quantification of enzymatic activities expressed as arbritary units fluorescent (AUF) in skin fibroblasts from control (C) and patient (P). Fluorimetric assay was started by the addition of specifics substrates Ala-Ala-Phe-NHMec /TPP1, 4-Methylumbelliferyl alpha-D-glucoside (GAA) 3-Acetylumbelliferyl beta-D-glucopyranoside/ (GBA) and Human beta-Galactosidase-1 (GLB1). Data are mean ± SD of five different determinations.

2.2.5 Mitochondrial respiration

To analyze the mitochondrial function in CLN5 disease, we performed measurements of OCR and ECAR in adherent fibroblasts (CLN5 mutant-derived fibroblasts) in real-time micro-oxygraphy with a XF96 Extracellular Flux Analyzer (Seahorse Bioscience, Billerica, MA). OCR was measured under basal conditions and in response to oligomycin, carbonylcyanide-4-(trifluoromethoxy)-phenylhydrazone (FCCP), Antimycin. The OCR measured under basal conditions (OCR-B), in response to oligomycin (OCR-O), and FCCP (OCR-F) did not show differences in patient's cells compared to control's fibroblasts (Fig. 14A-B). The same results were obtained when we considered the ratio between ECAR/OCR (Fig. 15A). Morover the amount of total mitochondrial ATP in the presence of 2-deoxy-Dglucose to block glycolysis in CLN5 patient's cells (c.335G>A/p.R112H and c.595C>T /p.R99*) was compared to wild-type fibroblasts. All these results indicated the absence of mitochondrial functional alteration in the CLN5 disease (Fig.15B).

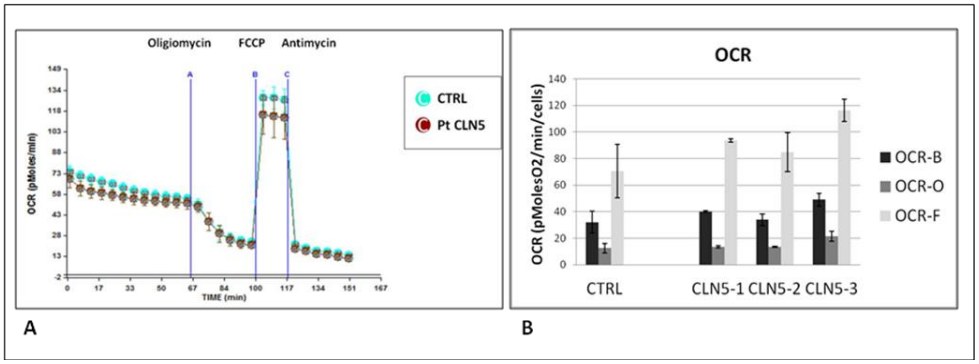

Figure 14. Panel A shows a representative the graph of oxygen consumption (OCR) in different conditions in control and mutant cell line. As expected, OCR in basal conditions (OCR-B) is inhibited when ATP synthesis is blocked by oligomycin(OCR-O),whereas is stimulated when oxidation is uncoupled from phosphorylation by FCCP (OCR-F). OCR Traces, expressed as pMolesO $_2$/min. CLN5-1: c.335G>A/p.R112H CLN5-2: c.595C>T/p.R99*, CLN5-3: c.788T>A /p.V263Q.The histogram in panel B reports the normalization of these data to the number of cells/well, expressed as mean values± SD of 12 replicates/cell line.

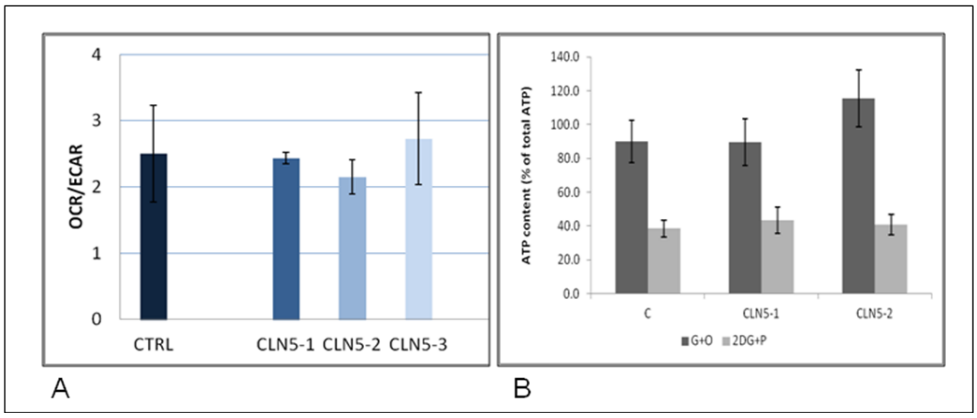

Figure 15. Panel A shows analysis of OCR/ECAR in basal conditions. CLN5-1: c.335G>A/p.R112H CLN5-2: c.595C>T /p.R99*, CLN5-3: c.788 T>A /p.V263Q. In panel B we indicated cells incubated 2 hrs in ATP record buffer supplemented with 10 mM glucose (Glu), 2.5 mg/mL oligomycin (Oligo), and 5 mM 2-deoxy-D-glucose plus 5 mM pyruvate (2GD+Pyr).

*2.3 Impairment of cell autophagy in primary CTSF/*CLN13 *cells*

We identified an Italian family with a vertical transmission of Type B KD where we detected a novel homozygous mutation in *CTSF*. The 42-year-old proposita presented tonic-clonic seizures since age 23, followed by development of cerebellar dysarthria and cognitive decline, finally evolving in frank dementia at age 30. Her deceased mother, a maternal aunt and a nice also showed a highly similar neurological picture. Six members of this family had a neurological syndrome compatible with KD. The two instances of parent-to-child transmission (Fig. 16), suggesting a dominant form of dementia such as those observed in Parry disease (Williams et al. 2012; Velinoy et al., 2012) or in *PSEN1*-related early-onset Alzheimer disease (Schellenberg et al. 2012), constituted initial confounding factors in the ascertainment of the causative mutation. Careful clinical assessment of the patients, meticulous collection of family history (from local general practitioners and through direct interviews with senior family members), and recognition of the high degree of inbreeding in the isolated community of Fondi, a municipality in central Italy numbering approximately 40,000 inhabitants, were crucial in disclosing an autosomal recessive pattern of inheritance, and therefore in prompting us to consider the possibility of mutations in *CTSF*.

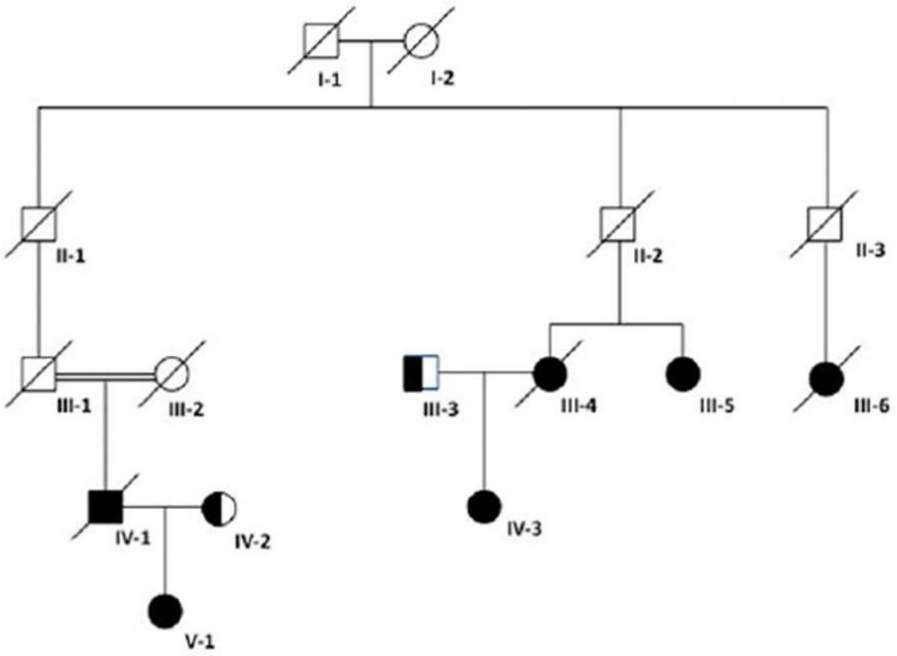

Figure 16. Family pedigree.

In subjects III-5, IV-3 and V-1 we detected a new homozygous c.213+1G>C mutation in *CTSF* (Fig. 17A). The mutation was heterozygous in eight asymptomatic relatives and excluded in large polymorphic databases (including dbSNP and Exome Sequence Variant). In cultured skin fibroblasts from the proposita and her maternal aunt, the mutation resulted in reduced *CTSF*/mRNA levels with incorrect splicing removing exon 1 and predicting a downstream starting codon with a chopped N-terminus of cathepsin F and a probable loss of function mechanism (Fig. 17B-C).

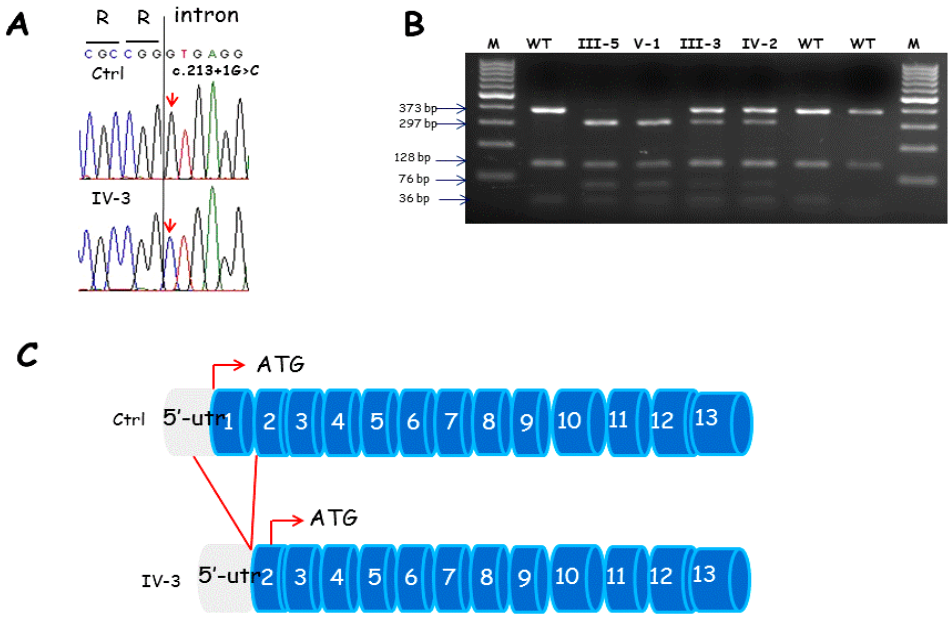

Figure 17. Molecular Analysis **A**. Sequencing results of control (Ctrl) and an affected individual (IV-3). Electropherograms of donor splice site region of the exon 1 of *CTSF* flanking the homozygous mutation identified in patient IV-3 at position c.213+1G>C (arrow). The wild-type sequence in Ctrl is also shown. **B.** PCR-restriction fragment length polymorphism (PCR-RFLP) for a rapid detection of the c.213+1G>C mutation employed the endonuclease *Dde*I. Using flanking oligonucleotide primers, we PCR-amplified a 537-bp fragment. Cleavage with *Dde*I produced 373-, 128-, and 36-bp fragments, both in wild-type subjects and control (Ctrl). The presence of the homozygous mutation in subjects III-5 and V-1 introduced an additional site of cleavage and resulted in 297-, 128-, 76-, and 36-bp fragments. The pattern seen in obligate heterozygous individuals (III-3, IV-2) shows 373-, 297-, 128-, 76-, and 36-bp fragments. M, 100-bp DNA marker size. **C.** Sequencing results of cDNA from cultured skin fibroblasts from a control (Ctrl) and subject IV-3. Electropherograms show part of the *CTSF* transcript obtained using primers located in exon 1 (5'-ctggagggaggactcagg-3') and exon 4 (5'-agccatcttcacaggcaagt-3'). Contrary to Ctrl, subject IV-3 lost 264-bp corresponding to part of 5'-UTR and exon 1 as well as the canonical start codon. Thus, a new transcript is predicted where part of the 5'UTR region is directly joined to exon 2, there is a downstream ATG in exon 2, and the transcript is reduced in size.

Western blotting showed low cathepsin F expression in cultured cells and enhanced expression of p62, LC3II and ubiquitin protein, possibly indicating disturbed autophagic processes (Fig. 18A-C).

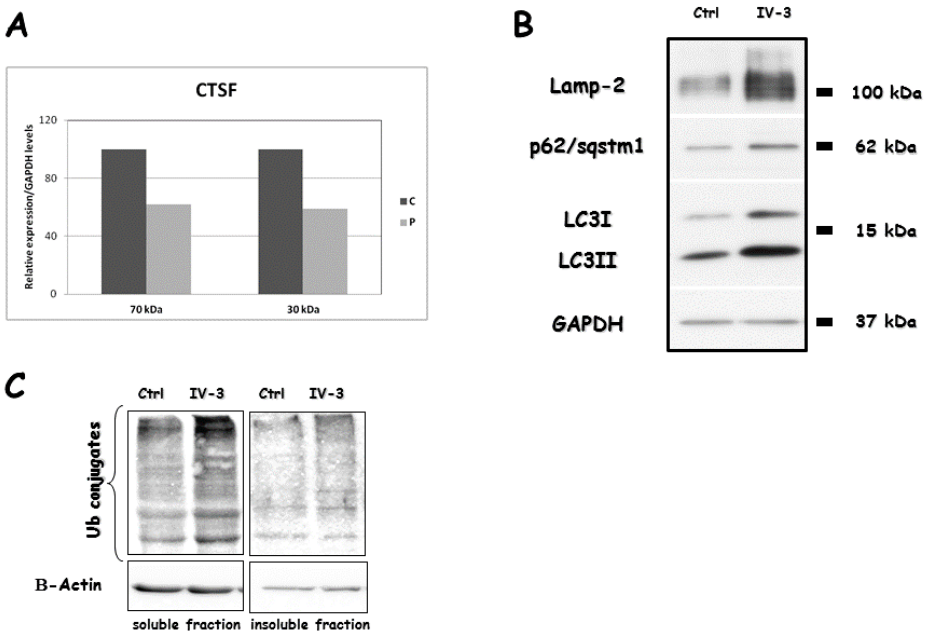

Figure 18. Protein Analysis. Representative Western blotting in cell lysates from patient IV-3 (P) and a control (C) analyzed for the indicated proteins. Glyceraldehyde 3-phosphate dehydrogenase (GAPDH) and β-actin were used as loading controls. A. Histogram showing a representative expression of human cathepsin F where a major band ~70 kDa and a minor band ~30 kDa were found to be reduced in IV-3 as compared to a normal control. B. Elevated content of LC3B, p62 and Lamp2 proteins is also evident in IV-3 when compared to the control. C. Ubiquitin expression was also increased in a soluble fraction of IV-3 cells.

Immunofluorescence on wild type fibroblasts showed a partial colocalization of CTSF and mitochondrial protein (Porin) (Fig. 19A). Aggresome formation was observed on patient's fibroblasts, using a novel red fluorescent molecular rotor dye, which is essentially non-fluorescent until it binds to the structural features associated with aggregated protein cargo. This was similar to observations made when autophagy was induced by treatment with the proteasome inhibitor MG 132 (Fig.19B).

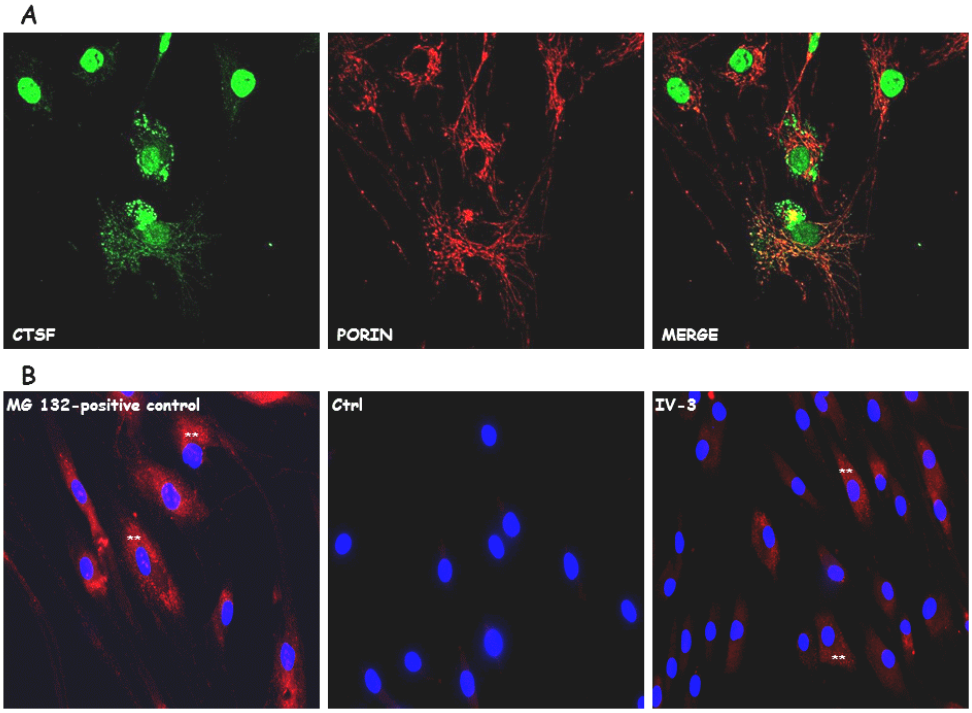

Figure 19. A. Confocal images (optical sections) showed intracellular cathepsin F (CTSF) (green fluorescence) and the mitochondrial marker Porin (red fluorescence). Merged images showed overlapping immunoreactivity in yellow. B. Aggresome formation as detected using the ProteoStat® aggresome detection dye (red fluorescence, **), and Hoechst 33342 nuclear stain (blue fluorescence). Cultured skin fibroblasts of patient IV-3 showed aggresome-like features (**) similar to control's cells that had been pre-treated with 5µM of MG-132, a proteasome inhibitor.

In Osmiophilic cytoplasmic inclusions suggestive of lipofucsin accumulation (aggresome-like structures) were seen ultrastructurally in skin biopsies from two patients (Fig. 20).

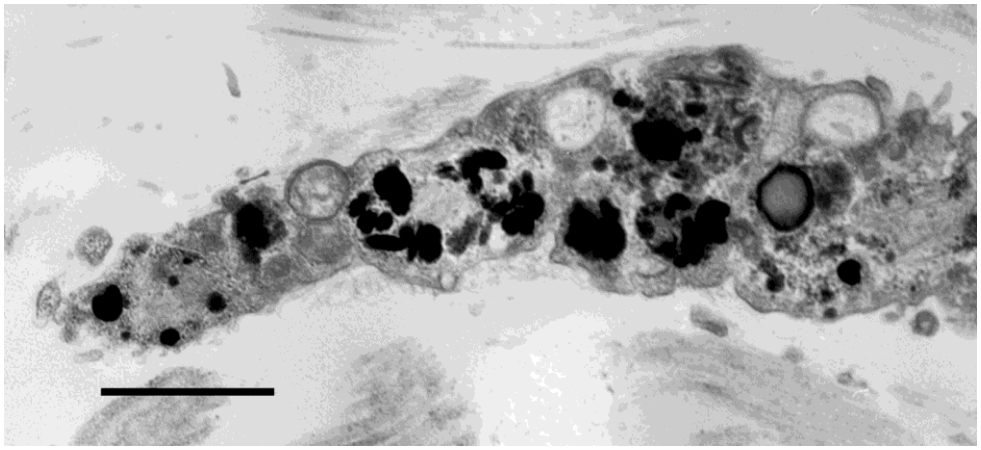

Figure 20. Electron microscopy of patient’s skin biopsy.

Discussion

The Neuronal Ceroid Lipofuscinoses (NCLs) represent a progressive group of inherited neurodegenerative diseases. Although the genetic underpinnings of most forms of NCL have been identified, the pathway(s) in which neuronal death results in the severe degenerative phenotype remain unknown, and there is no available rational basis for treatments. In this work we attempted to clarify the cellular and molecular mechanisms underlying three different forms of NCLs disease using patients' material and cell models. Our focus was on the identification of distinctive pathways that could characterize, at least in part, the diseases associated with different genes: *CLN1* (causing an Infantile type), *CLN5* (determining a Late Infantile form) and *CLN13-CTSF* (responsible for Adult-NCL) Our data indicate specific roles for the three affected proteins as follow.

The CLN1 protein (INCL) seems to be implicated in Oxidative metabolism pathways

We analyzed the mitochondrial compartment in CLN1 deficient skin fibroblasts and in an *in vitro* system of human neuroblastoma cells, SH-SY5Y, reproducing the pathological features seen in "Mediterranean" mutations in *CLN1*. Mitochondrial morpho/functional analysis showed an involvement of the mitochondrial compartment in both cellular systems. Our data confirmed previous observations reporting abnormalities in number, morphology and intracellular localization pattern of mitochondria in pathological primary cell lines (Pezzini et al., 2011). Moreover, a similar phenotype was seen in a good cellular model with neuronal-like structure. Mitochondrial dysfunctions could be, thus, involved in the pathogenesis of NCLs implying that mechanisms such as oxidative stress or apoptosis-induced via mitochondrial pathway can occur in the brain of CLN1 patients and offers further support to the possibility that small nucleophilic and lysosomotropic molecules with anti-oxidant properties alone or in

combination with potent antioxidant might have beneficial effects on the neurodegenerative process of the disease.

In perspective, we will examine mitochondrial membrane potential, ROS levels in primary skin fibroblast and differentiated neuroblastoma cells in normal and stress-induced conditions (using galactose medium as metabolic stressor).

The CLN5 protein (LINCL) is a player in abnormal lipid metabolism

The CLN5 disease is a variant form of late-infantile NCL and the exact pathogenetic mechanisms leading gene mutation to cause the disease is still unclear. Clinical and neuropathological similarities in NCL disorders may result from functional redundancy or co-operation of different NCL proteins (Vesa et al., 2002; Sleat et al., 2006) and it is known that the addition of CLN8p (the product of an additional NCL gene) or CERS1 (ceramide synthase) in CLN5-deficient patient fibroblast cells brings correction to the pathological phenotype (El Haddad et al., 2012).

We demonstrated the molecular interaction between CLN5, other NCL proteins, several lysosomal hydrolases and ceramides in an in vitro cellular system. In particular we found novel interactions between the CLN5 protein and four ceramide synthases (CERS1, CERS2, CERSS4, and CERS5) that synthesize ceramides, central molecules of sphingolipid metabolism in mammalian cells. Alike CLN8, also CLN5 seems to reside in the ER compartment but the presence of CLN5p in the ER is independent of the CLN8p. Since CLN5 resides in the lumen of intracellular organelles, it appears that interaction between CLN5 and the transmembrane proteins must be mediated by the lumenal domains of these proteins. Our results confirmed that the ER is an important hub station for the function and/or trafficking of NCL proteins and that these role do not imply a direct connection with mitochondrial inner membrane or mitochondrial bioenergetics. These data foresee a deeper investigation of ceramides (levels, pathway of synthesis or both) in CLN5 disease, the possible connections with the activation of autophagy or mitophagy

pathways, and the ensuing consequences on sphingolipid and phospholipid metabolisms. Again these avenues could imply new opportunities to hypothesize drug targets.

The CLN13 protein (cathepsin F) has a key role in Autophagy mediated processes

We characterized at the cellular level a novel c.213+1G>C in *CTSF* associated with ANCL- KD Type B (*CLN13*). The mutation affects correct splicing, removing exon 1 and predicting a chopped N-terminus of cathepsin F, with a probable loss-of-function mechanism. Overexpression of N-terminus truncated forms of human cathepsin F (Δ-CtsF) in HEK 293T cells has recently been associated with features suggestive of aggresome-like inclusions (Jerič et al., 2013) and multifunctional polyubiquitinated proteins. We demonstrated in CTSF hypofunctioning primary cells from three CLN13 patients ultrastructural features resembling aggresome-like structures in skin biopsies. These features were biochemically replicated in cultured fibroblasts, where we observed an increase of autophagic proteins highly reminiscent of what had been seen in HEK 293T cells (Jerič et al., 2013). All these results were suggestive of dysregulated autophagy, and points to an as yet unexplored connection between autophagy, proteasomal dysfunction and polyUb proteins in triggering neuronal cell death in adult-forms of NCL.

In a larger perspective, our data suggest that the common themes often claimed in the broad groups of NCL might be also distinguished at the cell levels at an extent that is not possible in murine models of the disease since those experimental system lack of the specificity offered by the human genetic background or point to mechanisms that are only partially applied in human NCL disease. Future approaches adopting also the 3-ome strategies could also impinge on these differences while searching novel therapeutic targets.

Conclusions

The NCL share clinical manifestations, biochemistry, and pathology, hence their classification together. NCL protein deficiencies result in similar cell biologic phenotypes including dysregulation of apoptosis and autophagy, prolonged inflammation, disturbed endoplasmic reticulum–cytosol calcium balance, impaired oxidative metabolism, and abnormal lipid trafficking. There are evidences that NCL proteins are essential components of a common pathway and that they may interact at multiple locations (Persaud-Sawin et al., 2007). It is possible to speculate on the possibility that a disruption in a common biological process leads to an NCL-disease. Yet, the possibility that individualized or specific mechanisms are more important in specific subtypes could offer more personalized approaches to cure.

To sum up, in this study we dissected at the cell level some of the specificities in three different forms of NCL pathology that are mostly relevant to Italian patients and our results pinpoint different steps in NCL disease and the involvement of specific cellular processes in the pathophysiological function of NCL proteins. The use of cell or model systems derived from affected individuals could also overcome some of the emerging conundrum of genetically-modified animal models where the pathogenic steps seem of discussed value in fully replicating the human pathology (Simonati et al, 2014). In perspective, all these steps and their specificities should be further explored to define steps more relevant as those might represent specific targets for developing more rationale therapeutic options.

Materials and Methods

4.1 Cell cultures and differentiation media

Human fibroblasts have been collected according to standard procedures from diagnostic skin biopsies.

Primary culture of human fibroblasts from:

1. Two patients harboring "Mediterranean" *CLN1* mutations. Patient 1 (Pt.1) was found to carry the homozygous c.665T>C mutation [p.L222P] whereas patient 2 (Pt.2) was compound heterozygous for the c.541G>T/c.124+1215_235-102del3.6Kb [p.V181L/p.A43_G145del].
2. CLN5 patients carrying different mutations in CLN5: c.788T>A/p.V263Q, c.335G>A/p.R112H and c.595C>T /p.R99*.

Moreover we used MEF (mouse embryonic fibroblasts) cells from wild type and CLN8 deficient ($Cln8^{-/-}$) mouse, HeLa cells from cervical tumor cells. The mouse model was generated in Dr Sardiello's laboratory at the Department of Human Genetics, Baylor College of Medicine, Houston (Texas).

3. CLN13 Patients' derived fibroblasts were obtained from punch biopsies of the affected individuals described in Di Fabio et al, 2014. A brief summary of clinical data of this novel form of adult-onset NCL is presented in Appendix.

All cell lines were grown at 37 °C with 5% CO2 in Dulbecco's modified Eagle's medium (DMEM), containing 10% fetal bovine serum (FBS), 4.5 g/L glucose and 1% antibiotics/antimycotics.

Neuroblastoma cell line SH SY5Y was cultured in DMEM/F12 1:1 with 10% FBS, 15 mM Hepes, L-glutamine, penicillin/streptomycin and amphotericin B (all purchased from Euroclone). Stable transfected clones were cultured in presence of 600 µg/ml G-418 (Geneticin, Euroclone). At 70-80% of confluence, cells were trypsinized and seeded at lower concentration (about one tenth). For neuronal differentiation, we set a 9

days long paradigm (hereafter referred as RA-NBM treatment) consisting in 2 phases: a 6 days pre-differentiation step in basal medium with 5% FBS and 10 μM *all trans* Retinoic Acid (RA, Sigma Aldrich) followed by a 3 days differentiation step in neurobasal medium (GIBCO, Life Technologies) enriched with 50 ng/ml recombinant human BDNF (rhBDNF, Peprotech), 2 mM dibutyril-cyclic AMP (dbcAMP, Sigma Aldrich), B27 Neuromix (Euroclone), 20 mM KCl, 1% L-glutamine (NBM). Briefly, 5000 cells per cm2 were seeded on flasks or alternatively on coverslips previously coated with ECMax gel (Sigma Aldrich), allowed to adhere for 24-48 hours and then exposed to basal or conditional media. Media were routinely changed every 2-3 days and the morphological features of the cultures were checked by phase contrast microscopy (Palomo et al., 2011).

4.2 Transfection

Transient transfection of wt and mutated cDNAs was performed in SH SY5Y cells. Stable transfected clones overexpressing the wt and different mutations of CLN1 cDNA are obtained after antibiotic selection with geneticin (G418, Gibco, LT) at 600 g/ml.

Molecular analysis and trasfection of neuroblastoma cells were performed in collaboration with the Unit of Molecular Medicine of Children Hospital "Bambino Gesù", Roma.

The protocols for the Lipofectamine LTX kit (Invitrogen) were followed for HeLa cells and the protocol of the Metafectene kit (Biontex Laboratories) was used for MEF cells.

4.3 Molecular analysis

The preparation of *CLN1* cDNAs (NM_000310) encoding wild-type (wt) and mutant (either c.125_235del or c.665T>C) inserted in pcDNA3 expression vector (Invitrogen, LT) were performed by standard PCR

methods. We confirmed the sequence both wt and mutated *CLN1* plasmids, by direct sequencing, using the BigDye Terminator v3.1 Cycle Sequencing Kit (Applied Biosystems, Foster City, CA) on an ABI3130xl automatic DNA Analyzer.

The *CTSF*/CLN13 gene was analyzed in peripheral blood DNA by PCR amplification and direct sequencing using BigDye 3.1 chemistry (Applied Biosystems, Foster City, CA, USA) and intronic oligonucleotide primers flanking the coding exons (sequences are available upon request). Gene deletions/duplications were excluded by the multiplex amplicon quantification (MAQ) technique. Nomenclature of mutations followed the guidelines of the Human Genome Variation Society (http://www.hgvs.org/mutnomen) and refers to the cDNA sequence (Genbank reference sequence version NM_003793.3) with the A of the translation initiation codon as +1.

We searched for all possible new single nucleotide variants (SNVs) both in a large set of in-house control chromosomes and in the dbSNP and Exome Variant databases (respectively http://www.ncbi.nlm.nih.gov/projects/SNP/ and http://evs.gs.washington.edu/EVS). New SNVs were also systematically evaluated *in silico* to predict their effects on protein function by means of Mutation Taster (http://www.mutationtaster.org/), Condel (http://bg.upf.edu/condel/), Polyphen analysis (http://genetics.bwh.harvard.edu/pph2/index.shtml) and ESEfinder (rulai.cshl.edu/new_alt_exon_db2/HTML/score.html and www.fruitfly.org /seq_tools/splice.html). The c.213+1G>C mutation was ruled out in control alleles and segregation was checked for in the family by ad hoc mutation-specific PCR-restriction fragment length polymorphism analysis.

Total RNA was purified from cultured skin fibroblasts obtained from patients and age-matched normal controls using TriReagent (Sigma-Aldrich, Milan, Italy) and was reversely transcribed using the 1st Strand cDNA Synthesis Kit (Roche, Hamburg, Germany) according to the manufacturer's random primer protocol. The consequences of the

c.213+1G>C mutation on splicing were examined by RT-PCR using primers located in the 5'UTR and in exon 4.

Mutations in knon NCL genes had been excluded in patient IV-3 prior to testing *CTSF*.

4.4 Immunofuorescence assay

For immunofluorescence analysis, paraformaldehyde-fixed coverslip-grown fibroblasts in antigen retrieval buffer [0.1MTris, 5% (w/v) urea, pH 9.5] were heated at 95°C for 10 min, followed by 15 min treatment with 0.1% Triton X-100 at room temperature. Slides were then incubated overnight at 4°C with mouse monoclonal anti-porin (Mitosciences, Eugene, OR), mitochondrial marker, and a rabbit anti-human cathepsin F polyclonal antibody (Santa Cruz) and in the presence of 10% FBS.

Neuroblastoma cells were fixed in 4% paraformaldehyde (PFA) for 20 minutes at RT. Cells were incubated in blocking buffer (10% normal goat serum, 0.3% Triton in PBS,) for 1h and then incubated over-night with the following primary antibodies: antibodies: anti-PPT-1 (1:50, Sigma), anti-βIII tubulin (1:100, Rabbit- Cell Signal Technology), anti-SMI-31 (1:100, Covance), anti-NF160 KDa (clone BF10) mouse monoclonal (1:100, Boehringer Mannheim). For fluorescence inspection, we used anti-mouse IgG (AbCam, Cambridge, UK) secondary antibodies conjugated with Alexa Fluor 488 and 555 (Molecular Probes) as well as 4',6-diamidino-2-phenylindole (DAPI) for nuclear staining. Images were acquired by an AxioCam equipment using AxioVision 4.3 software (Carl Zeiss).

HeLa cells were fixed with 100% ice methanol for 10 min, MEF cells were fixed with 4% PFA for 20 min at room temperature (RT). Blocking in 0.1% saponin, 10% FBS in PBS 1h RT. Slides were then incubated overnight at 4°C with primary antibody (1:200) in blocking solution. Primary antibodies were the following anti-Lamp2 (Mouse, Santa Cruz), anti-Lamp1 (Rat, Santa Cruz), anti-GFP (Chicken, Abcam), anti-FLAG (Rabbit, Sigma), anti-Myc (mouse and Rabbit, Sigma), anti-PDI (Mouse, BD bioscience),

anti-GM 130 (Rabbit, Abcam). For fluorescence visualization, we used secondary antibodies conjugated with Alexa Fluor 555 and 488 goat-anti mouse IgG, goat-anti rabbit IgG, goat-anti Chicken IgG and goat-anti Rat IgG (Molecular Probes), as well as 4',6-diamidino-2-phenylindole (DAPI) for nuclear staining. Images were acquired by confocal microscope (Zeiss LSM 710).

4.5 Aggresome detection

Cellular aggresomes were detected using the ProteoStat® Aggresome Detection kit according to the manufacturer's instructions (Enzo LifeSciences, Lausanne, Switzerland). Cultured cells were grown on coverslips and incubated for 12 h with MG-132, a cell-permeable proteasome inhibitor (5μM), which was used as a positive control. The cells were then washed with PBS, fixed in 4% paraformaldehyde for 30 min at room temperature, and permeabilized in permeabilizing solution (0.5% Triton X-100, 3 mM EDTA, pH 8.0 in 1× assay buffer) with gentle shaking on ice for 30 min. After this step, the cells were washed again in PBS and stained using the ProteoStat® Aggresome Detection Reagent and Hoechst 33342 nuclear stain for 30 min at room temperature protected from the light. The aggresomes were visualized using a Zeiss AX10 inverted fluorescence microscope equipped with an AxioCam MRc5 camera. The images were processed using AxioVision rel 4.8 acquisition software (Zeiss).

4.6 SDS-PAGE and Western Blotting

For Western blotting (WB) analysis, cultured skin fibroblasts, neuroblastoma stable clones and trasfected HeLa cells, were collected at confluence, washed twice with PBS and then homogenized in RIPA buffer (150 mM NaCl, 50 mM Tris–HCl, 6 mM EDTA, 1% NP-40, 0.1% SDS,

0.5% deoxycolic acid, pH 8.0) containing inhibitors of proteases (Roche Diagnostics GmbH, Mannheim, Germany). The cells were disrupted by 1 h incubation on ice and centrifuged for 10 min at 16,000 ×g at 4°C. The supernatant (soluble fraction) was collected and either used immediately or stored at −20 °C for later use. The pellets (insoluble fraction) were solubilized in 50µl of 1% (v/v) SDS in PBS for 10 min at room temperature; then, following addition of 50µl RIPA buffer, they were sonicated for 10 s. A 12% denaturing gel was loaded with 30-50 µg proteins. Proteins were then electron-transferred to nylon membranes (purchased from Bio-Rad Laboratories, Hercules, CA); the membranes were blocked with TBS/0.1% Tween20 (TTBS) containing 10% non-fat dry milk and then subjected to immunoblotting analysis. Primary antibodies were incubated overnight at 4°C in TTBS with 5% non-fat dry milk, and those not bound specifically were removed by washing in TTBS. Peroxidase-conjugated anti-mouse and anti-rabbit were used as secondary antibody (Jackson ImmunoResearch, laboratories Inc.) were added for 1 hour at room temperature in the same buffer as used for the primary antibodies (5% non-fat dry milk in TTBS). Reactive bands were detected using Immobilon Western Chemiluminescent HRP Substrate (Millipore Corporation, Billerica, MA), according to the manufacturer's instructions.

Quantitative blot analysis was performed using ImageJ software (http://rsbweb.nih.gov/ij/).

The primary antibodies used for WB analysis were:

1. Mitochondrial OXPHOS complexes: NDUFS3(30 kDa), SDHA (70 kDa), Core protein 2, COXII, CVα. VDAC/Porin, as a control for protein loading; (1:1000, Mitosciences, Eugene, OR, USA). Anti-GAPDH (1:10000, Abcam) and anti-βIII tubulin (1:1000, Cell Signal Technology).
2. Anti-FLAG mouse (1:5000, Sigma), anti-GFP mouse (1:1000, Roche Applied Science) and anti-Myc rabbit (1:1000, Sigma).
3. Anti-cathepsin F (1:500; Santa Cruz Biotechnology, Heidelberg, Germany), monoclonal anti-Lamp2 (1:8000; H4B4 clone Abcam,

Cambridge, UK), polyclonal anti-LC3II (1:2000; Cell Signalling Technology, Santa Clara, California), anti-ubiquitin (1:500, Dako, Beverley, MA), and monoclonal anti- p62/sqstm1 (1:2000; BD Biosciences, Oxford, UK). Monoclonal mouse anti-β-actin (1:50.000; Sigma-Aldrich) and rabbit polyclonal anti-GAPDH (1:10,000; Sigma-Aldrich) were employed as loading controls.

4.7 Mitochondrial Protein Preparation

Mitochondrial pellets were isolated from cell cultures as described elsewhere (Calvaruso et al.,2008). Briefly, fibroblasts were cultured until cells were70% confluent. Cells were harvested with trypsin, washed twice with phosphate-buffered saline (PBS), and re-suspended in 100 µl PBS plus 100 ml of digitonin solution (4 mg/ml). The cell solution was kept on ice for 10 min to dissolve the membranes. One milliliter of cold PBS was added to the cells, which were spun for 10 min at 10 000 r.p.m. at 4C. The supernatant was removed, the pellet washed one more time in 1 ml cold PBS, and the protein concentration was determined using the BCA protein assay kit (Pierce). For the preparation of native mitochondrial complexes, pellets were solubilized in 100µl buffer containing 1.5M aminocaproic acid, 50 mM Bis – Tris, pH 7.0. Next, 1% (w/v)n-dodecyl b-D-maltoside was added and solubilized samples were incubated on ice for 15min and centrifuged for 30 min at 13,000 rpm at 4° C, and the supernatant was combined with 10µl of sample buffer (750 mM aminocaproic acid, 50 mMBis – Tris, 0.5 mM EDTA, 5% Serva Blue G-250) prior to loading.
antibodies.

4.8 Blue Native Analysis

Blue native 3 – 13% gradient gels were loaded with 60µg of mitochondrial protein using 50 mM Bis – Tris as an anode buffer and 15 mM Bis –

Tris/50 mM tricine containing 0.02% Serva Blue G-250 as a cathode buffer. After electrophoresis, proteins were transferred to a PVDF membrane at 35 V, overnight, and probed with specific antibodies (proteins were subjected to Western blotting. Duplicate gels were further used for in-gel activity (IGA) assays.

4.9 IGA assay

In-gel activity assays entail the incubation of the gels in complex specific-solutions that contain substrates and color reagents which stain upon the acceptance of electrons or phosphate. Because the OXPHOS complexes are native they still have enzymatic activity. Combination of the appearing stained bands and their molecular weight allow good and quantitative identification of the individual complexes. Gels are incubated at room temperature with the following solutions: Complex I: 5 mM Tris–HCl, pH 7.4, 0.1 mg/ml NADH, and 2.5 mg/ml NTB (NitroTetrazolium Blue, Sigma).Complex IV: 50 mM sodium phosphate buffer, pH 7.2, 0.5 mg/ml 3.3' -diamidobenzidine tetrahydrochloride (DAB, Sigma–Aldrich) 0.05 mM cytochrome c (horse heart <95% purity, Sigma).

4.10 Total and mitochondrial ATP assay

ATP levels were measured using the Luminescence ATP Detection Assay System (ATPlite one step, PerkinElmer Life Sciences). Briefly, $1x10^4$ and $3x10^4$, respectively for cultured fibroblasts and SH-SY5Y cells, were used and they were seeded in a 96-well plate (1×10^4 cells/well) and incubated in 10% FBS/DMEM medium for 48 h. After discarding the medium, cells were washed with ATP record buffer (156mM NaCl, 3mM KCl, 2 mM MgSO4, 1.25mM KH2PO4, 2 mM CaCl2, 20mM HEPES, pH 7.35) and incubated for 2 h in buffer with either 10 mM glucose, 10 mM glucose plus 2.5 μg/ml oligomycin (glycolytic ATP generation), or 5 mM 2-deoxy-

Dglucose plus 5 mM pyruvate (oxidative ATP production) (Nogueira et al., 2013).

Then cells were incubated with the luciferin/luciferase reagent and ATP production in samples was measured using an Orion L Microplate Luminometer (Berthold Detection Systems GmbH).

4.11 Transmission electron microscopy

Specimens from skin biopsies were fixed in 2.5% glutaraldehyde in 100 mM phosphate buffer for 3 hours at 4°C. After washing in buffer, samples were the post-fixed in 1% osmium tetraoxide for 2 hours at 4 °C, dehydrated by increasing concentrations of acetone and subsequently embedded in Spurr resin. Ultra-thin slices were cut by microtome, stained in uranyl acetate and lead citrate and finally observed under the EM 109 electron microscope (Carl Zeiss, Munich Germany).

4.12 Cloning

We created construct plasmid expression vectors, using the appropriate vectors, by fusing the sequences encoding the selected protein fragments (YFP - yellow fluorescent protein, Myc and FLAG) with the sequences encoding the proteins of interest.

We generated linearized expression vectors (p3XFLAG-CMVTM-13-Sigma, pcDNA 3./cmyc- His A-Invitrogen, MCFD2-YFPC and YFPN-ERGIC 53) using restriction endonucleases (*Not*1, *BamH*1, *Hind*III, *EcoR*I, *Cla*I and *Xho*I; New England Biolabs); then we gel purified the linearized vector using Gel Ectraction kit (Qiagen). For the directional cloning of one fragment of DNA into the vectors we used the In-Fusion HD Cloning Kit (Clontech® Laboratories, Inc.), this method permits to fuse DNA fragments (e.g. PCR-generated sequences and linearized vectors), efficiently and precisely by recognizing a 15 base pairs (bp) overlap at their

ends. This 15-bp overlap can be engineered by designing primers for amplification of the desired sequences (Tab. 2).

Gene	*Sense primer*	*Antisense primer*
YFP-CLN5	5' CAGTGTGGTGGAATTCATGCGCCGGAACCTGCGC 3'	5'CCACCGCCACCATCGATTAAACCAGAGAGTGTTTGTTTCTGATAGG 3'
CLN5-YFP	5' GGTGGGTCCGCTCGAGTTCCCTCCCGGCGCCACT 3'	5' GCCCTCTAGACTCGAGTTATAAACCAGAGAGTGTTTGTTTCTGATAGG 3'
YFP-CERS1	5' GGTGGGTCCGCTCGAGTTATGGCGGCGGCGGGGGC 3'	5' GCCCTCTAGACTCGAGTCAGAAGCGCTTGTCCTTCACCAGGCC 3'
CERS1-YFP	5' CAGTGTGGTGGAATTCATGGCGGCGGCGGGGCCC 3'	5' CCACCGCCACCATCGATGAAGCGCTTGTCCTTCACCAGGCCGTT 3'
YFP-CERS2	5' GGTGGGTCCGCTCGAGTTATGCTCCAGACCTTGTATGATT 3'	5' GCCCTCTAGACTCGAGTCAGTCATTCTTACGATGGTTGTT 3'
CERS2-YFP	5' CAGTGTGGTGGAATTCATGCTCCAGACCTTGTATGATTAC 3'	5' CCACCGCCACCATCGATGTCATTCTTACGATGGTTGTTATTGA 3'
YFP-CERS4	5' GGTGGGTCCGCTCGAGTTATGCTGTCCAGTTTCAACGAGT 3'	5' GCCCTCTAGACTCGAGCTATGTGGCTGTTGTGTGCCTGTT 3'
CERS4-YFP	5' CAGTGTGGTGGAATTCATGCTGTCCAGTTTCAACGAGTGG 3'	5' CCACCGCCACCATCGATTGTGGCTGTTGTGTGCCTGTT 3'
YFP-CERS5	5' GGTGGGTCCGCTCGAGTTATGGCGACAGCAGCGC 3'	5' GCCCTCTAGACTCGAGTTACTCTTCAGCCCAGTAGCTGCC 3'
CERS5-YFP	5' CAGTGTGGTGGAATTCATGGCGACAGCAGCGC 3'	5' CCACCGCCACCATCGATCTCTTCAGCCCAGTAGCTGC 3'
YFP-CERS6	5' GGTGGGTCCGCTCGAGTTATGGCAGGGATCTTAGCCTG 3'	5' CCTGCCATAACTCGAGTTAATCATCCATGGAGCAGGAGCC 3'
CERS6-YFP	5' CAGTGTGGTGGAATTCATGGCAGGGATCTTAGCCTG 3'	5' CCACCGCCACCATCGATATCATCCATGGAGCAGGAGCC 3'

Table 2. Primers used for the designing constructs YFPN-YFPC of the *CLN5*, *CERS1, CERS2, CERS4, CERS5, CERS6* genes.

We amplified the genes of interest using CloneAmp HiFi PCR Premix: (conditions were 35 cycles of 98°C 10 sec, 63°C 10sec, 72°C 1 min). The purified PCR fragment was fused with the linearized vector in the in-Fusion cloning reaction and incubated for 1h at 50°C. Afterward we cotransformed Stellar competent cells using standard method of heat shock with the plasmids containing the fusions and plated them on ampicillin (AmpR) selective LB plates. We incubated all plates overnight at 37°C. The following day we picked individual isolated colonies from each experimental plate. To determine the presence of insert, we isolated plasmid DNA using a mini prep kit (Pure Link TM Quick Plasmid Miniprep Kit, Invitrogen), analyzed the DNA by restriction digestion or colony PCR screening (SapphireAMP Fast PCR master mix, Clontech® Laboratories, Inc.), and confirmed the presence of insert by sequencing (Fig.21)

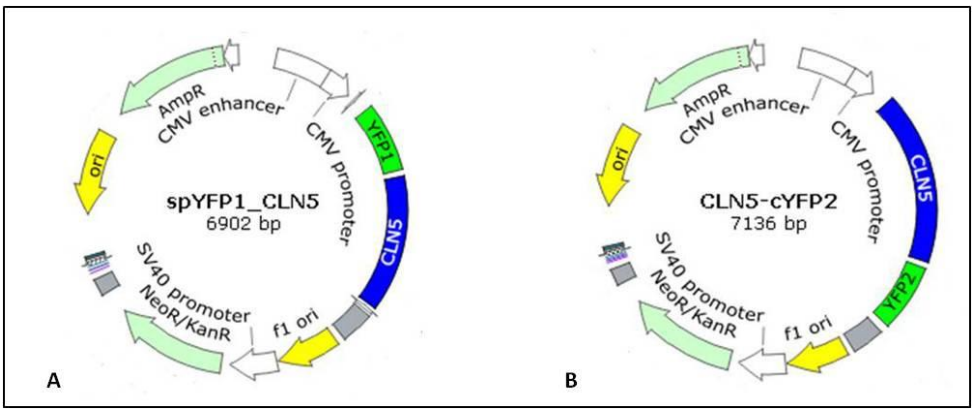

Figure 21. Protein fusion vectors. Plasmid maps of vectors encoding the protein fusions CLN5-NYFP (inserted in the plasmid ERIGC53) and CLN5-CYFP (inserted inthe plasmid MCFD2)

Cells were transfected with different cDNA-vector constructs.

4.13 Bimolecular fluorescence complementation (BiFC) analyses

The BiFC assay is based on two non-fluorescent fragments of a fluorescent protein which, when fused to two interacting proteins, yield fluorescence due to the stable formation of a functional fluorescent protein inside the cell. The analysis was performed as previously described (Kerpolla et al., 2008) (Fig.22).

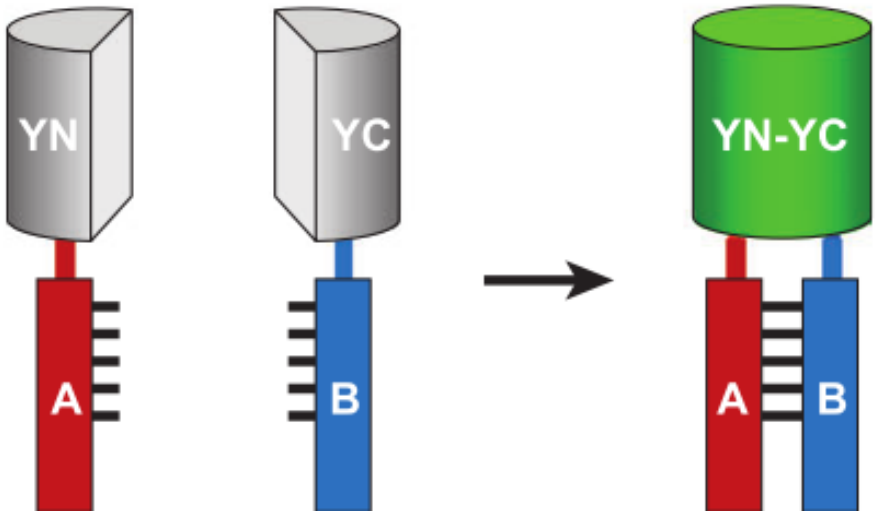

Figure 22. Schematic representation of the principle of the BiFC assay. Two nonfluorescent fragments (YN and YC) of the yellow fluorescent protein (YFP) are fused to putative interaction partners (A and B). The association of the interaction partners allows formation of a bimolecular fluorescent complex.

Protein fusion vectors: YFP N-terminal fragment (Y1), YFP C-terminal fragment (Y2), (Tab.2). The library of lysosomal proteins constructs was generated in the laboratory of Dr Sardiello, Department of Human Genetics, Baylor College of Medicine, Houston (Texas) (Tab.3).

Table 3. Library of lysosomal proteins for BiFC constructs (YN-YC)

ACP5	acid Phosphatase 5 Tartrate Resistant	***GNS***	glucosamine (N-acetyl)-6-sulfatase
AGA	aspartylglucosaminidase	***GUSB***	beta glucuronidase
ARSA	arylsulfatase A	***HEXB***	hexosaminidase B
ARSB	arylsulfatase B	***HPSE***	Heparanase
ARSG	arylsulfatase G	***HYAL1***	hyaluronoglucosaminidase 1
ARSK	arylsulfatase K	***IDS***	iduronate 2-sulfatase
ASAH1	N-acylsphingosine amidohydrolase	***MAN2B1***	mannosidase alpha class 1B
CTBS	Chitobiase, Di-N-Acetyl	***MAN2B2***	mannosidase, alpha, class 2B
CTSA	cathepsin A	***MANBA***	mannosidase beta A
CTSB	cathepsin B	***MPO***	Myeloperoxidase
CTSC	cathepsin C	***NAAA***	N-acylethanolamine acid amidase
CTSD	cathepsin D	***NAGA***	N-acetylgalactosaminidase, alpha-
CTSF	cathepsin F	***NAGLU***	N-acetylglucosaminidase alpha
CTSH	cathepsin H	***NEU1***	sialidase 1
CTSK	cathepsin K	***NPC2***	Niemann-Pick disease, type C2
CTSO	cathepsin O	***PCYOX1***	prenylcysteine oxidase 1
CTSS	cathepsin S	***PLA2G15***	phospholipase A2, group XV
CTSZ	cathepsin Z	***PLBD2***	phospholipase B domain containing 2
DNAS2	deoxyribonuclease II	***PPT2***	palmitoyl-protein thioesterase
ERGIC53	ER-Golgi intermediate compartment	***PSAP***	Prosaposin
FUCA1	fucosidase, alpha-L- 1	***RNASET2***	ribonuclease T2
GAA	glucosidase alpha acid	***SCARB2***	lysosomal membrane sialoglycoprotein
GALC	galactosylceramidase	***SCPEP1***	serine carboxypeptidase 1
GALNS	galactosamine (N-acetyl)-6-sulfate	***SGSH***	N-sulfoglucosamine sulfohydrolase
GBA	Glucosidase beta acid	***SIAE***	sialic acid acetylesterase
GGH	gamma-glutamyl hydrolase	***SMPD1***	sphingomyelin phosphodiesterase 1
GLA	gamma-carboxyglutamic acid	***TPP1***	tripeptidyl peptidase I
GLB1	Galactosidase beta 1	***PPT1***	palmitoyl-protein thioesterase 1
GM2A	GM2 ganglioside activator	***CLN8***	ceroid lipofuscinosis, neuronal, 8

For microscopy: $1x10^4$ HeLa cells/well in 8-chamber slides were transfected with 500 ng of total DNA. Cells were visualized on confocal microscope (Zeiss LSM 710) 24h after the transfection in PBS buffer. The microscope equipped with a camera (or similar equipment) at a magnification of 20X. To visualize the YFP, used as a reporter protein, a

filter for GFP excitation (450–495 nm) and a GFP emission filter (515–560 nm) were required.

For flow cytometric we plated $8x10^4$ Hela cells/well in 24-well chamber with 600 ng of total DNA. To quantify the efficiency of fluorescence complementation, it was necessary to include an internal control in the experiment to normalize for differences in transfection efficiency and the level of protein expression. For this purpose, cells were cotransfected with plasmids encoding the two fusion proteins (e.g., fused to YFPN and YFPC), together with a plasmid encoding a full-length fluorescent protein with distinct spectral characteristics (peseudo-colored red, CFP). Cells transfected were analyzed after 48h, resuspended cells in 1%FBS/PBS. Flow cytometry was performed using a BD LSRFortessa cell analyzer (BD Biosciences). The fluorescence intensities produced by both BiFC (YN-YC) and the internal control (CFP, cells transfected) were measured in individual cells. The ratio of YN-YC to CFP emission was calculated after subtraction of background signal (negative control-pCDNA). The ratio of YN-YC to CFP fluorescence is a measure of the efficiency of BiFC. The ratios for different structurally related fusion proteins can reflect the relative efficiencies of complex formation (the positive interaction) in living cells (Fig.23).

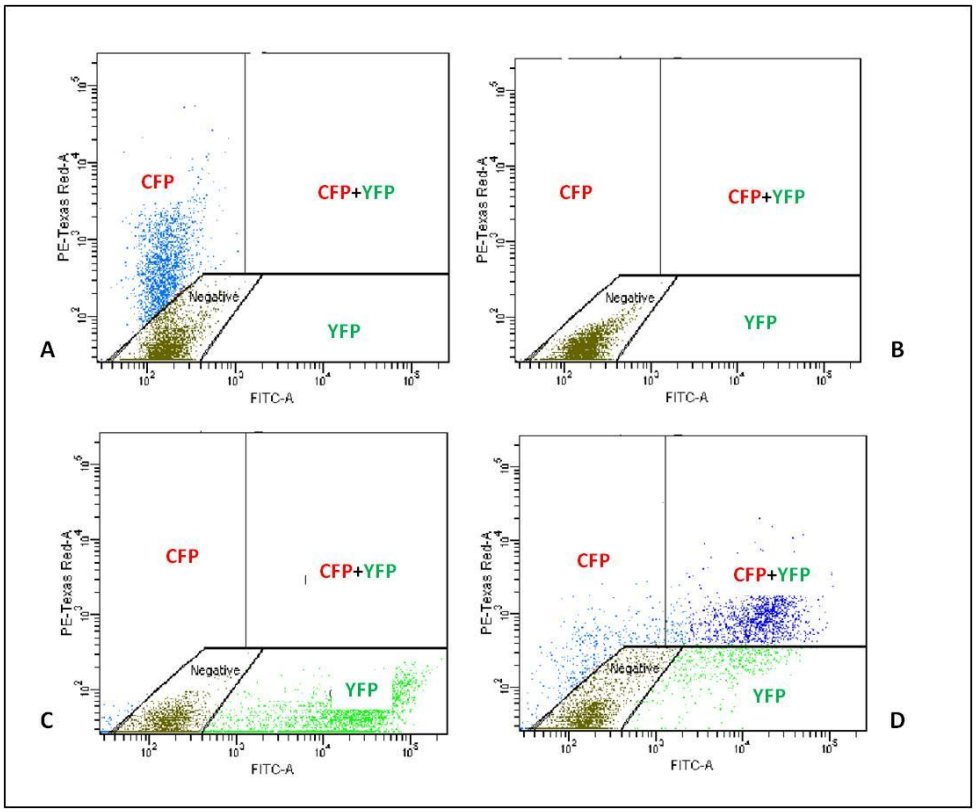

Figure 23. Flow cytometry: Gating for flow cytometry analysis of fluorescent protein expressing in HeLa cells. A) CFP protein (Red signal) B) pcDNA (negative control-no signal) C) YFP protein (Green signal) D) CFP+YFP (Red-Green) cells positive for the interaction.

4.14 Co-immunoprecipitation

HeLa cells, 60 mm^2 ($1.2x10^6$ cells) dishes were co-transfected with a total of 7.5 mg of DNA that included: plasmid encoding FLAG- CERS1 and CLN8 proteins, plasmid encoding a CLN5 Myc and YFP- CERS proteins (CERS2, CERS4, CERS5 and CERS6). A variable amount of DNA was transfected for particular constructs to ensure similar levels of expression. About 48 h after transfection, cells were lysed with 1.0% Nonidet P-40 buffer (50 mM Tris, pH 7.5, 150 mM NaCl, 10% glycerol, 1 mM DTT, EDTA-free protease inhibitor pellets (Roche Applied Science). 200 μg of total protein from transfected Hela cells were used for individual coIP experiments. Lysates were incubated with primary antibody for 30 min and precipitated for 4 h with 10 μl of protein G agarose (Roche Applied

Science) at 4 °C. FLAG proteins were immunoprecipitated and immunoblotted with a mouse monoclonal anti-FLAG antibody (1:5000, Sigma). GFP fusion proteins were precipitated and immunoblotted with a mouse monoclonal anti-GFP antibody (1:1000, Roche Applied Science). Myc protein was immunoprecipitated and immunoblotted with a rabbit polyclonal anti-Myc antibody (1:1000, Sigma). Samples were run on SDS-PAGE, 4 –12% Bis-Tris gel (Invitrogen) immunoblotted with indicated antibodies and visualized with HRP-conjugated anti-mouse or anti-rabbit secondary antibodies, detected using ECL chemiluninescence for immunodetection.

4.15 Enzyme activity assays

Fibroblasts were seeded in a 96-well plate (1 x 10^4 cells/well) and incubated in 10% FBS/DMEM medium for 24 h. After discarding the medium, cells were incubated in 0.2 M acetate buffer (pH 4.5) containing 0.1% Triton X-100 (v/v). Fluorimetric assay was started by the addition of specifics substrates Ala-Ala-Phe-NHMec (Sigma)/TPP1 (Vines et al., 1999), 4-Methylumbelliferyl alpha-D-glucoside (Sigma)/Glucosidase alpha acid (GAA) (Wen Yang et al., 1998), 3-Acetylumbelliferyl beta-D-glucopyranoside (Sigma)/ Glucosidase beta acid (GBA) (Song et al., 2013) and Human beta-Galactosidase-1 (R&D system)/Galactosidase beta 1 (GLB1) (Brunetti-Pierri et al., 2009). Reactions were incubated at 37°C for 2-6 hrs. Fluorescence was measured (excitation 360 nm, emission 460 nm) with a Gen5 microplate reader (BioTek Instruments).

4.16 OCR and ECAR measurements

Oxygen consumption rate (OCR) and extra-cellular acidification rate (ECAR) were measured in adherent fibroblasts with a XF96 Extracellular Flux Analyzer (Seahorse Bioscience, Billerica, MA, USA). Each control and mutant fibroblast cell lines were plated in XF 96-well cell culture

microplates at a density of 2.5–7.5 × 10^3 cells/well in in 200 μL of DMEM and incubated for 24 h at 37 °C in 5% CO_2 atmosphere. After replacing the growth medium with 175 μL of XF media (non-buffered DMEM medium, containing 5 mM glucose, 0.5 mM L-glutamine, ph 7.62), pre-warmed at 37°C cells were preincubated for 30 min. before starting the assay procedure. After baseline measurements of OCR (OCR-B) and ECAR, OCR was measured after sequentially adding to each well oligomycin and carbonyl cyanide 4-(trifluoromethoxy) phenylhy-drazone (FCCP), to reach working concentrations of 1μg/ml and 0.4 μM, respectively. We evaluated the fraction of non-mitochondrial oxygen consumption, by measuring OCR after complete inhibition of the mitochondrial respiratory chain with antimycin 1 μM (all chemical were from Sigma Aldrich) (Invernizzi et al. 2012).

Statistical analysis and data processing

The mean+SEM values of at least three independent experiments are represented in the figures. Statistical comparison of the data sets was performed using Student's t-test. The differences are presented with their corresponding statistical significance or P-value.

Acknowledgments

The study has been performed in the Department of Neurological, Psycological, Morfological and Motor Sciences, University of Verona Medical School, Laboratory of "Developmental Neuropathology" (Prof. A. Simonati); in collaboration with the Division of Molecular Medicine, IRCSS "Fondazione Stella Maris", University of Pisa (Dr. F.M. Santorelli) and Department of Molecular and Human Genetics, Baylor College of Medicine, Houston-Texas, USA (Dr. M. Sardiello). We thank Dr. Marzia Bianchi, Unit of Molecular Medicine of Children Hospital "Bambino Gesù" (Roma, Italy) who collaborated in the molecular analyses and trasfection of neuroblastoma cells. We also acknowledge the contribution

of Dr. Francesco Pezzini, Department of Neurological, Psycological, Morfological and Motor Sciences, University of Verona Medical School, Laboratory of “Developmental Neuropathology" who collaborated in the neuronal differentiation.

We are grateful to Dr. Marco Sardiello and his staff members for guiding me throughout some experimental steps and the kind gift of a library of lysosomal protein constructs and $Cln8^{-/-}$ murine cells.

The study was strenuously supported by the Italian National Association of Neuronal Ceroid Lipofuscinosis (A-NCL).

References

Ahtiainen L, Luiro K, Kauppi M, Tyynelä J, Kopra O, Jalanko A, Palmitoyl protein thioesterase 1 (PPT1) deficiency causes endocytic defects connected to abnormal saposin processing. Exp. Cell Res. 2006; 312: 1540–1553.

Ahtiainen L, Van Diggelen O P, Jalanko A, Kopra O. Palmitoyl protein thioesterase 1 is targeted to the axons in neurons. J. Comp. Neurol. 2003; 455: 368–377.

Anderson GW, Goebel HH, Simonati A. Human pathology in NCL. Biochim Biophys Acta. 2013; 1832: 1807-26.

Bellizzi JJ, Widom J, Kemp C, Lu JY, Das AK, Hofmann SL, Clardy J. The crystal structure of palmitoyl protein thioesterase 1 and the molecular basis of infantile neuronal ceroid lipofuscinosis. Proc. Natl. Acad. Sci. U. S. A. 2000; 4573–4578.

Bible E, Gupta P, et al. Regional and cellular neuropathology in the palmitoyl protein thioesterase-1 null mutant mouse model of infantile neuronal ceroid lipofuscinosis. Neurobiol. Dis. 2004; 16: 346–359.

Blom T, Schmiedt ML, Wong AM, Kyttälä A, Soronen J, Jauhiainen M, Tyynelä J, Cooper JD, Jalanko A. Exacerbated neuronal ceroid lipofuscinosis phenotype in Cln1/5 double-knockout mice. Dis Model Mech. 2013; 6: 342-57.

Boustany RM Lysosomal storage diseases--the horizon expands. Nat Rev Neurol. 2013; 9: 583-98.

Brunetti-Pierri N, Scaglia F.Mol Genet Metab. GM1 gangliosidosis: review of clinical, molecular, and therapeutic aspects. 2008; 94: 391-6.

Calvaruso MA, Smeitink J, Nijtmans L. Electrophoresis techniques to investigate defects in oxidative phosphorylation. Methods. 2008; 46: 281-7.

Camp LA, Verkruyse LA, Afendis SJ,. Slaughter CA,. Hofmann SL. Molecular Cloning and expression of palmitoyl-protein thioesterase. J.Biol. Chem. 1994; 269: 23212–23219.

Cho S, Dawson G. Palmitoyl protein thioesterase 1 protects against apoptosis mediated by Ras–Akt–caspase pathway in neuroblastoma cells. J. Neurochem. 2000; 74: 1478–1488.

Cho S, Dawson PE., Dawson G. Antisense palmitoyl protein thioesterase 1 (PPT1) treatment inhibits PPT1 activity and increases cell death in LA-N-5 neuroblastoma cells. J. Neurosci. Res. 2000; 62: 234–240.

Das AK, Lu JY, Hofmann SL. Biochemical analysis of mutations in palmitoyl protein thioesterase causing infantile and late-onset forms of neuronal ceroid lipofuscinosis. Hum. Mol. Genet. 2001; 10: 1431–1439.

Das AM, Jolly RD, Kohlschütter A. Anomalies of mitochondrial ATP synthase regulation in four different types of neuronal ceroid lipofuscinosis. Mol. Genet. Metab. 1999; 66: 349–355.

Di Fabio R, Moro F, Pestillo L, Meschini MC, Pezzini F, Doccini S, Casali C, Pierelli F, Simonati A, Santorelli FM. Pseudo-dominant inheritance of a novel CTSF mutation associated with type B Kufs disease. Neurology 2014; 83: 1769-70.

Goswami R, Ahmed M, Kilkus J, Han T, Dawson SA, Dawson G. Differential regulation of ceramide in lipid-rich microdomains (rafts): antagonistic role of palmitoyl:protein thioesterase and neutral sphingomyelinase 2. J. Neurosci. Res. 2005; 81: 208–217.

Griffey M, Macauley SL, et al.. AAV2-mediated ocular gene therapy for infantile neuronal ceroid lipofuscinosis. Mol. Ther. 2005; 12: 413–421.

Gupta P, Soyombo AA, et al. Disruption of PPT1 or PPT2 causes neuronal ceroid lipofuscinosis in knockout mice. Proc. Natl. Acad. Sci. U. S. A. 2001; 98: 13566–13571.

Groh J, Kühl TG, Ip CW, Nelvagal HR, Sri S, Duckett S, Mirza M, Langmann T, Cooper JD, Martini R. Immune cells perturb axons and impair neuronal survival in a mouse model of infantile neuronal ceroid lipofuscinosis. Brain. 2013; 136: 1083-101.

Haddad SE, Khoury M, Daoud M, Kantar R, Harati H, Mousallem T, Alzate O, Meyer B, Boustany RM. CLN5 and CLN8 protein association with ceramide synthase: biochemical and proteomic approaches. Electrophoresis. 2012; 33: 3798-809.

Haltia,M, Rapola,J and Santavuori P. Infantiletypeofso-called neuronal ceroid-lipofuscinosis. Histological and electron microscopic studies. Acta Neuropathol. 1973; 26: 157–170.

Hawkins-Salsbury JA, Cooper JD, Sands MS. Pathogenesis and therapies for infantile neuronal ceroid lipofuscinosis (infantile CLN1disease). Biochim Biophys Acta. 2013; 1832: 1906-9.

Heinonen O, Kyttälä A, Lehmus E, Paunio T, Peltonen L, Jalanko A. Expression of palmitoyl protein thioesterase in neurons, Mol. Genet. Metab. 2000; 69: 123–129.

Hermansson M, Käkelä R, Berghall M, Lehesjoki AE, Somerharju P, Lahtinen U. Mass spectrometric analysis reveals changes in phospholipid, neutral sphingolipid and sulfatide molecular species in progressive epilepsy with mental retardation, EPMR, brain: a case study. J. Neurochem. 2005; 95: 609–617.

Holmberg V, Jalanko A, Isosomppi J, Fabritius AL, Peltonen L, Kopra O. The mouse ortholog of the neuronal ceroid lipofuscinosis CLN5gene encodes a soluble lysosomal glycoprotein expressed in the developing brain. Neurobiol.Dis. 2004; 16: 29–40.

Holmberg V, Lauronen L, Autti T, Santavuori P, Savukoski M, Uvebrant P, Hofman I, Peltonen L, J¨arvel¨a I. Phenotype-genotype correlation in eight patients with Finnish variant late infantile NCL (CLN5). Neurology 2000; 55: 579–581.

Invernizzi F, D'Amato I, Jensen PB, Ravaglia S, Zeviani M, Tiranti V. Microscale oxygraphy reveals OXPHOS impairment in MRC mutant cells. Mitochondrion. 2012; 12: 328-35.

Isosomppi J, Vesa J, Jalanko A, Peltonen L. Lysosomal localization of the neuronal ceroid lipofuscinosis CLN5 protein. Hum Mol Genet. 2002; 11: 885–891.

Isosomppi J, Heinonen O, Hiltunen JO, Greene ND, Vesa, J, Uusitalo A, Mitchison HM, Saarma M, Jalanko A, Peltonen L. Developmental expression of palmitoyl protein thioesterase in normal mice. Brain Res. Dev. Brain Res. 1999; 118: 1–11.

Jalanko A, Vesa J, Manninen T, von Schantz C, Minye H, Fabritius AL, Salonen T, Rapola J, Gentile M, Kopra O, Peltonen L. Mice with Ppt1Deltaex4 mutation replicate the INCL phenotype and show an inflammation-associated loss of interneurons. Neurobiol. Dis. 2005; 18: 226–241.

Jerič B, Dolenc I, Mihelič M, et al. N-terminally truncated forms of human cathepsin F accumulate in aggresome-like inclusions. Biochim Biophys Acta 2013; 1833: 2254-2266.

Kerppola TK. Bimolecular fluorescence complementation: visualization of molecular interactions in living cells. Methods Cell Biol. 2008; 85: 431-70.

Kim SJ, Zhang Z, Hitomi E, Lee YC,. Mukherjee AB. Endoplasmic reticulum stress-induced caspase-4 activation mediates apoptosis and neurodegeneration in INCL. Hum. Mol. Genet. 2006; 15: 1826–1834.

Kim S.J., Zhang Z., Lee Y.C., Mukherjee A.B. Palmitoyl-protein thioesterase-1 deficiency leads to the activation of caspase-9 and contributes to rapid neurodegeneration in INCL, Hum. Mol. Genet. 2006; 15: 1580–1586.

Kollmann K, Mutenda KE, Balleininger M, Eckermann E, von Figura K, Schmidt B, Lübke T, Identification of novel lysosomal matrix proteins by proteome analysis. Proteomics. 2005; 5: 3966–3978.

Kopra O, Vesa J, von Schantz C, Manninen T, Minye H,. Fabritius AL, Rapola J, van Diggelen OP, Saarela J, Jalanko A, Peltonen L. A mouse model for Finnish variant late infantile neuronal ceroid lipofuscinosis,

CLN5, reveals neuropathology associated with early aging. Hum. Mol. Genet. 2004; 13: 2893–2906.

Lebrun AH, Storch S, Ruschendorf F, Schmiedt ML, Kyttälä A,. Mole SE, Kitzmüller C, Saar K,. Mewasingh LD,. Boda V, Kohlschütter A, Ullrich K, Braulke T, Schulz A. Retention of lysosomal protein CLN5 in the endoplasmic reticulum causes neuronal ceroid lipofuscinosis in Asian sibship. Hum. Mutat. 2009; 30: E651–661.

Lehtovirta M, Kyttälä A, Eskelinen EL, Hess M, Heinonen O, Jalanko A. Palmitoyl protein thioesterase (PPT) localizes into synaptosomes and synaptic vesicles in neurons: implications for infantile neuronal ceroid lipofuscinosis (INCL). Hum. Mol. Genet. 2001; 10: 69–75.

Levy M, Futerman AH. Mammalian ceramide synthases. IUBMB Life. 2010; 62: 347-56.

Lieberman AP, Puertollano R, Raben N, Slaugenhaupt S, Walkley SU, Ballabio A. Autophagy in lysosomal storage disorders. Autophagy. 2012; 8: 719-30.

Lindstedt L, Lee M, Oorni K, Bromme D, Kovanen PT. Cathepsins F and S block HDL3-induced cholesterol efflux from macrophage foam cells. Biochem. Biophys. Res. Commun. 2003; 312: 1019–1024.

Lyly A, von Schantz C, Salonen T, Kopra O, Saarela J, Jauhiainen M, Kyttälä A, Jalanko A. Glycosylation, transport, and complex formation of palmitoyl protein thioesterase 1 (PPT1)—distinct characteristics in neurons. BMC Cell Biol. 2007; 8: 22.

Mamo A, Jules F, Dumaresq-Doiron K, Costantino S, Lefrancois S. The role of ceroid lipofuscinosis neuronal protein 5 (CLN5) in endosomal sorting. Mol. Cell. Biol. 2012; 32: 1855–1866.

Mancini C, Nassani S, Guo Y, Chen Y, Giorgio E, Brussino A, Di Gregorio E, Cavalieri S, Lo Buono N, Funaro A, Pizio NR, Nmezi B, Kyttala A, Santorelli FM, Padiath QS,Hakonarson H, Zhang H, Brusco A. Adult-onset autosomal recessive ataxia associated with neuronal ceroid lipofuscinosis type 5 gene (CLN5) mutations. J Neurol. 2015; 262: 173-8.

Nogueira C, Meschini MC, Nesti C, Garcia P, Diogo L, Valongo C, Costa R, Videira A, Vilarinho L, Santorelli FM. A Novel SUCLA2 Mutation in a Portuguese Child Associated With "Mild" Methylmalonic Aciduria. J Child Neurol. 2015; 30: 228-32.

Ohno K, Saito S, Sugawara K, Suzuki T, Togawa T, Sakuraba H. Structural basis of neuronal ceroid lipofuscinosis 1. Brain Dev. 2010; 32: 524–530.

Oörni K, Sneck M, Bromme D,. Pentikainen MO, Lindstedt KA, Mayranpaa M, Aitio H, Kovanen PT. Cysteine protease cathepsin F is expressed in human atherosclerotic lesions, is secreted by cultured macrophages, and modifies low density lipoprotein particles in vitro. J.Biol.Chem. 2004; 279: 34776–34784.

Palomo GM, Cerrato T, Gargini R, Diaz-Nido J. Silencing of frataxin gene expression triggers p53dependent apoptosis in human neuron-like cells. Hum Mol Genet. 2011; 20: 2807-22.

Pérez-Poyato MS, Milà Recansens M, Ferrer Abizanda I, Montero Sánchez R, Rodríguez-Revenga L, Cusí Sánchez V, García González MM, Domingo Jiménez R, Camino León R,Velázquez Fragua R, Martínez-Bermejo A, Pineda Marfà M. Juvenile neuronal ceroid lipofuscinosis: clinical course and genetic studies in Spanish patients. J Inherit Metab Dis. 2011; 34: 1083-93.

Persaud-Sawin DA, Mousallem T, Wang C, Zucker A, Kominami E, Boustany RM. Neuronal ceroid lipofuscinosis: a common pathway? Pediatr Res. 2007; 61: 146-52.

Peters J, Rittger A, Weisner R, Knabbe J, Zunke F, Rothaug M, Damme M, Berkovic SF, Blanz J, Saftig P, Schwake M. Lysosomal integral membrane protein type-2 (LIMP-2/SCARB2) is a substrate of cathepsin-F, a cysteine protease mutated in type-B-Kufs-disease. Biochem Biophys Res Commun. 2015; 457: 334-40.

Pezzini F, Gismondi F, Tessa A, Tonin P, Carrozzo R, Mole SE , Santorelli FM, Simonati A. Involvement of the mitochondrial compartment

in human NCL fibroblasts. Biochem. Biophys. Res. Commun. 2011; 416: 159–164.

Porter MY, Turmaine M, Mole SE. Identification and characterization of Caenorhabditis elegans palmitoyl protein thioesterase1, J. Neurosci. Res. 2005; 79: 836–848.

Ramadan H, Al-Din AS, Ismail A, Balen F, Varma A, Twomey A, Watts R, Jackson M, Anderson G, Green E, Mole SE. Adult neuronal ceroid lipofuscinosis caused by deficiency in palmitoyl protein thioesterase 1. 2007; 68: 387-8.

Santamaria I., Velasco G., Pendas A.M., Paz A., Lopez-Otin C.. Molecular cloning and structural and functional characterization of human cathepsin F, a new cysteine proteinase of the papain family with a long propeptide domain, J. Biol. Chem. 1999; 274: 13800–13809.

Santavuori P, Rapola J, Nuutila A, Raininko R, Lappi M, Launes J, Herva R, Sainio K. The spectrum of jansky-bielschowsky disease. Neuropediatrics 1991; 22: 92–96.

Santavuori P, Rapola J, Raininko R, Autti T, Lappi M, Nuutila A, Launes J, Sainio K. Early juvenile neuronal ceroid-lipofuscinos is or variant jansky-bielschowsky disease:Diagnostic criteria and nomenclature. J. Inherit Metab. Dis.1993; 16: 230–232.

Santavuori P, Rapola J, Sainio K, Raitta C. A variant of jansky-bielschowsky disease. Neuropediatrics.1982; 13: 135–141.

Santorelli FM, Bertini E, Petruzzella V, Di Capua M, Calvieri S, Gasparini P, and Zeviani M. A Novel Insertion Mutation (A169i) in the CLN1 Gene Is Associated with Infantile Neuronal Ceroid Lipofuscinosis in an Italian Patient. Biochemical and biophysical research communications. 1998; 245: 519–522.

Santorelli FM, Garavaglia B, Cardona F, Nardocci N, Bernardina BD, Sartori S, Suppiej A, Bertini E, Claps D, Battini R, Biancheri R, Filocamo M, Pezzini F, Simonati A. Molecular epidemiology of childhood neuronal ceroid-lipofuscinosis in Italy. Orphanet J Rare Dis. 2013; 2: 8-19.

Savukoski M, Klockars T, Holmberg V, Santavuori P, Lander ES, Peltonen L. CLN5, a novel gene encoding a putative transmembrane protein mutated in Finnish variant late infantile neuronal ceroid lipofuscinosis. Nat. Genet. 1998; 19: 286–288.

Schellenberg GD, Montine TJ. The genetics and neuropathology of Alzheimer's disease. Acta Neuropathol 2012; 124: 305-323.

Schmiedt ML, Blom T, Kopra O, Wong A, von Schantz-Fant C, Ikonen E, Kuronen M, Jauhiainen M, Cooper JD, Jalanko A, Cln5-deficiency in mice leads to microglial activation, defective myelination and changes in lipid metabolism.Neurobiol. Dis. 2012; 46: 19–29.

Schmiedt ML, Bessa C, Heine C, Gil Ribeiro M, Jalanko A, Kyttälä A. The neuronal ceroid lipofuscinosis protein CLN5: New insights into cellular maturation, transport and consequences of mutations. Hum Mutat. 2010; 31: 356-65.

Schulz, A, Mousallem, T, Venkataramani M, PersaudSawin, DA, Zucker, A, Luberto C, Bielawska A, Bielawski J, Holthuis JC, Jazwinski SM, Kozhaya L, Dbaibo GS, Boustany, RM. J. Biol. Chem. 2006; 281: 2784–2794.

Sentelle RD, Senkal CE, Jiang W, Ponnusamy S, Gencer S, Selvam SP, Ramshesh VK, Peterson YK, Lemasters JJ, Szulc ZM, Bielawski J, Ogretmen B. Ceramide targets autophagosomes to mitochondria and induces lethal mitophagy. Nat Chem Biol. 2012; 8: 831-8.

Shi GP, Bryant RA, Riese R, Verhelst S, Driessen C, Li Z, Bromme D, Ploegh HL, Chapman HA. Role for cathepsin F in invariant chain processing and major histocompatibility complex class II peptide loading by macrophages, J. Exp. Med. 2000; 191: 1177–1186.

Simonati A, Tessa A, Bernardina BD, Biancheri R, Veneselli E, Tozzi G, Bonsignore M, Grosso S, Piemonte F, Santorelli FM. Variant late infantile neuronal ceroid lipofuscinosis because of CLN1 mutations. Pediatr Neurol. 2009; 40: 271-6.

Simonati A, Pezzini F, Moro F, Santorelli FM. Neuronal Ceroid Lipofuscinosis: The Increasing Spectrum of an Old Disease. Curr Mol Med. 2014 Oct 10. [Epub ahead of print].

Sleat DE, Zheng H, Qian M, Lobel P. Identification of sites of mannose 6-phosphorylationon lysosomal proteins. Mol. Cell. Proteomics 2006; 5: 686–701.

Smith KR, Dahl HH, Canafoglia L, Andermann E, Damiano J, Morbin M, Bruni AC, Giaccone G, Cossette P, Saftig P, Grötzinger J, Schwake M, Andermann F,Staropoli JF, Sims KB, Mole SE, Franceschetti S, Alexander NA, Cooper JD, Chapman HA, Carpenter S, Berkovic SF, Bahlo M. Cathepsin F mutations cause Type B Kufs disease, an adult-onset neuronal ceroid lipofuscinosis. Hum Mol Genet. 2013; 22: 1417-23.

Song W, Wang F, Savini M, Ake A, di Ronza A, Sardiello M, Segatori L.TFEB regulates lysosomal proteostasis. Hum Mol Genet. 2013; 22: 1994-2009.

Tang CH, Lee JW, Galvez MG, Robillard L, Mole SE., Chapman HA. Murine cathepsin F deficiency causes neuronal lipofuscinosis and late-onset neurological disease. Mol. Cell. Biol. 2006; 26: 2309–2316.

Tyynelä J, Suopanki J, Baumann M, Haltia M. Sphingolipid activator proteins (SAPs) in neuronal ceroid lipofuscinoses (NCL). Neuropediatrics 1997; 28: 49–52.

Vanni N, Fruscione F, Ferlazzo E, Striano P, Robbiano A, Traverso M, Sander T, Falace A, Gazzerro E, Bramanti P, Bielawski J, Fassio A, Minetti C, Genton P, Zara F. Impairment of ceramide synthesis causes a novel progressive myoclonus epilepsy. Ann Neurol. 2014; 76: 206-12.

Velinov M, Dolzhanskaya N, Gonzalez M, et al. Mutations in the gene DNAJC5 cause autosomal dominant Kufs disease in a proportion of cases: study of the Parry family and 8 other families. PLoS One 2012; 7: e29729.

Vesa J, Hellsten E, Verkruyse LA, Camp LA, Rapola J, Santavuori P, Hofmann SL, Peltonen L. Mutations in the palmitoyl protein thioesterase gene causing infantile neuronal ceroid lipofuscinosis. Nature 1995; 376: 584-7.

Vesa J, Chin MH, Oelgeschläger K, Isosomppi J, DellAngelica EC, Jalanko A, Peltonen L. Neuronal ceroid lipofuscinoses are connected at molecular level: interaction of CLN5 protein with CLN2 and CLN3. Mol. Biol. Cell. 2002; 13: 2410–2420.

Vines DJ, Warburton MJ. Classical late infantile neuronal ceroid lipofuscinosis fibroblasts are deficient in lysosomal tripeptidyl peptidase I. FEBS Lett. 1999 ;443: 1 31-5.

Virmani T, Gupta P, Liu X, Kavalali ET, Hofmann SL. Progressively reduced synaptic vesicle pool size in cultured neurons derived from neuronal ceroid lipofuscinosis-1 knockout mice. Neurobiol. Dis. 2005; 20: 314–323.

Wang B, Shi GP, Yao PM, Li Z, Chapman HA, Bromme D. Human cathepsin F Molecular cloning, functional expression, tissue localization, and enzymatic characterization. J. Biol. Chem. 1998; 273: 32000–32008.

Wei H, Zhang Z, Saha A, Peng S, Chandra G, Quezado Z,. Mukherjee AB. Disruption of adaptive energy metabolism and elevated ribosomal p-S6K1 levels contribute to INCL pathogenesis: partial rescue by resveratrol. Hum. Mol. Genet. 2011; 20: 1111–1121.

Wen Yang H, Kikuchi T, Hagiwara Y, Mizutani M, Chen YT and Van Hove JLK. Recombinant Human Acid α-Glucosidase Corrects Acidα-Glucosidase-Deficient Human Fibroblasts, Quail Fibroblasts, and Quail Myoblasts. Pediatric Research 1998; 43: 374–380.

Wex T, Wex H, Bromme D. The human cathepsin F gene a fusion product between an ancestral cathepsin and cystatin gene. Biol.Chem. 1999; 380: 1439–1442.

Williams RE, Mole SE. New nomenclature and classification scheme for the neuronal ceroid lipofuscinoses. Neurology. 2012; 79: 183-91.

Zhang Z, Butler JD, Levin SW, Wisniewski KE, Brooks SS., Mukherjee AB. Lysosomal ceroid depletion by drugs: therapeutic implications for a hereditary neurodegenerative disease of childhood. Nat. Med. 2001; 7: 478–484.

Zhang Z, Lee YC, Kim SJ, Choi MS, Tsai PC, Xu Y, Xiao YJ, Zhang P, Heffer A, Mukherjee AB. Palmitoyl-protein thioesterase-1 deficiency mediates the activation of the unfolded protein response and neuronal apoptosis in INCL. Hum. Mol. Genet. 2006; 15: 337–346.

Appendix

Patients CTSF

The proposita (IV-3), a 42 years old when first seen by us, is a woman who, at age 23 years, presented clusters of tonic-clonic seizures, fully controlled by a combination of sodium valproate (1250 mg/day) and carbamazepine (1200 mg/day). Her medical history was only remarkable for mild head traumas that occurred at age 28 years. From the age of 30, she showed a progressive cognitive decline. She rapidly became aphasic and displayed suprabulbar signs. Her relatives reported sporadic lower limb myoclonic jerks. In recent years neurological examination had revealed transient facial dyskinesias, which had first appeared several years after the onset of the cognitive impairment. A brain MRI at 36 years showed severe cortical and cerebellar atrophy and diffuse periventricular hyperintensity in T2-weighted sequences. At age 40, the patient became wheelchair-bound and totally dependent on caregivers for activities of daily living. The patient has since developed axial hypotonia, postural tremor in the upper limbs, brisk deep tendon reflexes and bilateral Babinski sign associated with frontal release signs. Her vision is preserved.

Her mother (case III-4) experienced tonic-clonic seizures since the age of 25. She subsequently displayed behavioral disturbances, emotional lability and, from age 35, intellectual deterioration. At age 52, her mental deterioration accelerated rapidly, finally resulting in a clinical diagnosis of severe cognitive impairment. She died at the age of 56.

Patient III-5, now 74 years old, is a woman who, at the age of 32, suffered a minor head trauma. At 66, she suffered a second head trauma, without significant consequences (brain CT was normal). At the age of 69, her cognition began to decline. On her most recent neurological examination, at the age of 73, she was confined to a wheelchair, aphasic and presented severe dementia. Postural tremor in the upper limbs was detected as well

action myoclonus and perioral dyskinesias. Reduced deep tendon reflexes, primitive reflexes and bilateral Babinski were also observed.

Patient V-1, 45 years old, is a woman who has experienced occasional tonic-clonic seizures since age 21. At age 39, she had a head trauma with minor sequelae. Afterwards, she developed rapidly progressive cognitive decline, initially evident only in housework, but later also in social relationships. Her most recent neurological examination showed cerebellar dysarthria, occasional dysphasia with confabulation, ideomotor apraxia, inappropriate laughing, and urinary incontinence. A brain MRI showed severe cortical atrophy.

Patient IV-1, deceased, was a man with severe dementia that had begun when he was 55 years old. At age 48, he had undergone a neurological examination because he had experienced tonic-clonic seizures. He died at age 67.

No clinical records are available for patient III-6, a woman who reportedly had several episodes of generalized epilepsy starting at age 8 years, after a febrile episode. Relatives reported that she had experienced rapidly progressive intellectual decline culminating in frank dementia. Albeit presenting some gait impairment, she apparently walked autonomously until her death at age 50 years during an acute episode of massive rhabdomyolysis.